PARTICLES AND COSMOLOGY

17th Baksan School
on Astroparticle Physics

STUDENT PROJECTS

Razvilka Cheget, Terskol, Kabardino-Balkarian Republic, Russia

3-11 April 2025

CONTENTS

Project 1. ***One Neutrino to Bring Them All. What Can We Learn from the KM3NeT Extreme-Energy Event?*** **3**
I INTRODUCTION . . . 3
II DETECTOR MODELS . . . 3
III ISOTROPIC FLUX MODEL . . . 5
IV CONCLUSIONS . . . 6

Project 3. ***TXS 0506–056 as a neutrino source. What can be derived from IceCube and Baikal-GVD observations?*** **7**
I SIGNAL MODEL DEFINITION . . . 7
II BACKGROUND . . . 8
III DETECTOR MODEL . . . 9
IV OBSERVATION SIGNIFICANCE . . . 9
V SOURCE PARAMETERS ESTIMATION . . . 10
VI SUMMARY . . . 11

Project 4. ***Muon and Electron Signatures in Super–Kamiokande and Sensitivity to Proton Decay*** **13**
I ENERGY DEPOSITION DIFFERENCES . . . 13
II RANGE ESTIMATION IN MATTER . . . 15
III CONTAINMENT IN SK . . . 15
IV PROTON DECAY SIGNAL . . . 16
V PROTON LIFETIME SENSITIVITY . . . 16

Project 5. ***Production and Use of ^{18}F for Neutrino Detector Calibration*** **18**
I DESIGN OF THE ACTIVATION SETUP . . . 18
II DECAY PROPERTIES . . . 19
III DETECTOR RESPONSE MODELING . . . 19
IV CALIBRATION PRECISION . . . 20
V CONCLUSION . . . 21

Project 7. ***Solar Neutrinos, Tritium Background, and Dark Matter in XENON1T*** **22**
I INTRODUCTION . . . 22
II OBJECTIVES . . . 22
III SENSITIVITY TO ^{8}B SOLAR NEUTRINOS . . . 23
IV LOW-ENERGY EVENT EXCESS AND THE TRITIUM BACKGROUND 24
V DARK MATTER SEARCH . . . 24
VI SUMMARY . . . 25

Project 9. ***Lunar-Based Ultimate Neutrino Telescope*** **26**
I INTRODUCTION . . . 26
II DETECTION METHOD . . . 26
III OPTIMAL LOCATION AND GEOMETRY OF THE DETECTOR . . . 27
IV NEUTRINO FLUX CALCULATION . . . 28
V CONSTRUCTION PHASES AND EXPENDITURE BUDGET . . . 28
VI CONCLUSIONS . . . 28

Project 10. ***Can Earth's Atmosphere Serve as the Largest Neutrino Detector?*** **30**
I TASK 1: ATMOSPHERE VS WATER AS DETECTION MEDIUM . . . 30
II COMPARING NEUTRINO INTERACTION PROBABILITIES IN WATER VS. ATMOSPHERE . . . 31
III TASK 2: NEUTRINO AND GAMMA-RAY DETECTION MODES . . . 32

IV CONCLUSION 33
V OBSERVATIONAL SIGNATURES OF NEUTRINO AND GAMMA-RAY DETECTION MODES 33
VI COMPARISON TABLE OF OBSERVATIONAL SIGNATURES 34
VII TASK 3: RATE ESTIMATES 34
VIII COMPARISON WITH ICECUBE AND OTHER DETECTORS 35
IX TASK 4. MISSION DESIGN 36
X TASK 5. BUDGET AND PROPOSAL DEFENSE 36
XI SUMMARY OF THE PROPOSAL 37
XII CONCLUSION 38

One Neutrino to Bring Them All. What Can We Learn from the KM3NeT Extreme-Energy Event?

Maria Kalyashova[1], Nikita Pozdnukhov[2], Dmitry Salnikov[2],
Alexander Schepkin[3], Simon Sotirov[2], Nikita Vasiliev[4]

[1]*Ioffe Institute,* [2]*INR RAS,* [3]*ITMO University,* [4]*MSU*

Project Author:
Grigory Rubtsov,
INR RAS

Scientific Advisor:
Nickolay Martynenko,
MSU & INR RAS

Abstract

In February 2025, Nature published the observation of a neutrino with a record energy of 220 PeV by the KM3NeT experiment. At the same time, the IceCube experiment – with a significantly larger effective volume and exposure – has not reported any neutrinos with such high energies. What conclusions can be drawn about the nature of neutrino sources based on a single extreme-energy detection?

I. INTRODUCTION

In February 2025, the KM3NeT collaboration announced the observation of a neutrino with a record energy of 220 PeV [1] (the topography of the event can be seen at Fig. 1). At the same time, the IceCube experiment – with a significantly larger effective volume and exposure – has not reported any neutrinos with such high energies.

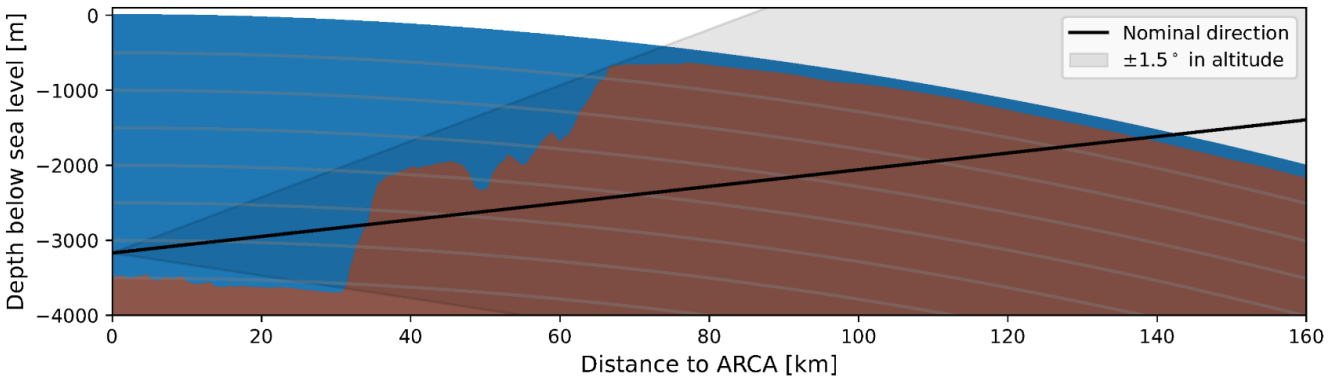

FIG. 1: Illustration of the KM3NeT event topography.

The project aims to evaluate the probability of such an outcome. We model detector efficiencies and effective areas, and obtain estimates of the neutrino flux in the isotropic flux model. We also perform a joint-fit analysis with the data from IceCube, both with non-detection in the $>$ 100 PeV range and with the data from the $\approx$ PeV region.

II. DETECTOR MODELS

The general idea of the detector model is as follows. We assume that the detector looks for Cherenkov light from high-energy muon tracks born in the interaction of muon neutrino with the Earth. Cherenkov light cone must reach the detector, so the muon must reach the point de-

fined by the angle of the Cherenkov cone. We assume an ad-hoc cutoff on the minimum energy of detected muons of 1 TeV. As the analysis deals with PeV neutrinos, this has no significant impact and partly accounts for detection efficiency. The length of the muon path is defined by the pair-production energy losses (see the school's lectures :)).

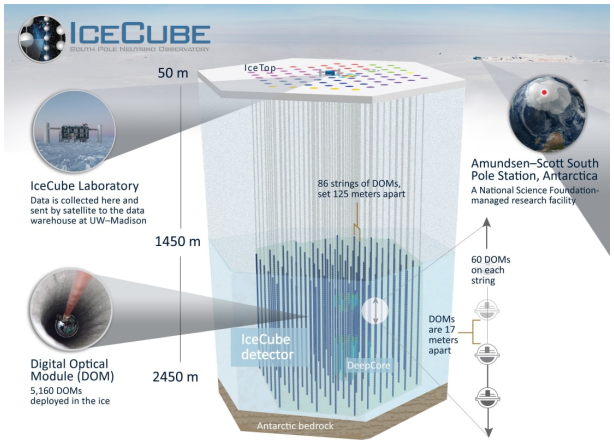

FIG. 2: IceCube geometry illustration.

$$-\frac{dE_\mu(\text{GeV})}{dx(\text{m})} = 0.5 \cdot 10^{-3} \times E_\mu(\text{GeV}). \quad (1)$$

Neutrino must interact with matter via the $\nu_\mu + p/n \to \mu + X$ process before the detector and closer than the maximum muon path. This gives us a simple analytical expression for detector efficiency:

$$\text{Eff} = \exp(-\sigma n(L - l_{max})) - \exp(-\sigma n L), \quad (2)$$

where L is the neutrino path to detector and l_{max} is the maximum muon path in matter. Neutrino interaction cross-sections are taken from [2]. We forgo the neutrino energy resolution entirely, as it is not as important for the flux analysis and very hard to estimate with any degree of accuracy due to light absorption in the medium and photomultiplier efficiency.

We then model the detector geometry and the neutrino path length, accounting for the different materials along the path (rock, water, and ice). The resulting dependence of detection efficiency on the incoming neutrino angles is presented in Fig. 3.

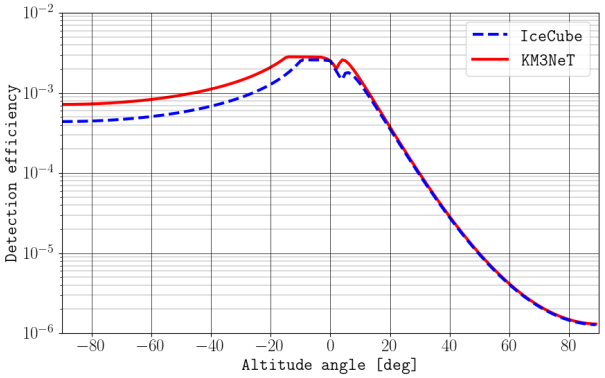

FIG. 3: Dependence of detection efficiency on altitude angle for both KM3NeT (solid red line), and IceCube (dashed blue line) experiments. Energy is fixed at 100 PeV.

We also present the effective area dependence on neutrino energy for both the KM3NeT and IceCube detectors (Fig. 4), as well as a comparison with the real KM3NeT effective area (Fig. 5) taken from the open collaboration data.

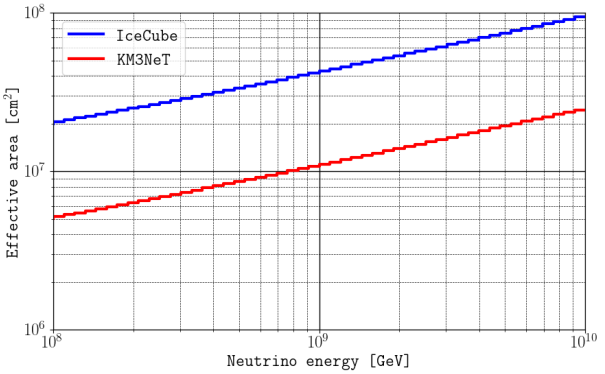

FIG. 4: Naive estimation of KM3NeT and IceCube effective areas with respect to muon neutrinos. The red line and the blue lines correspond to the KM3NeT and IceCube, respectively.

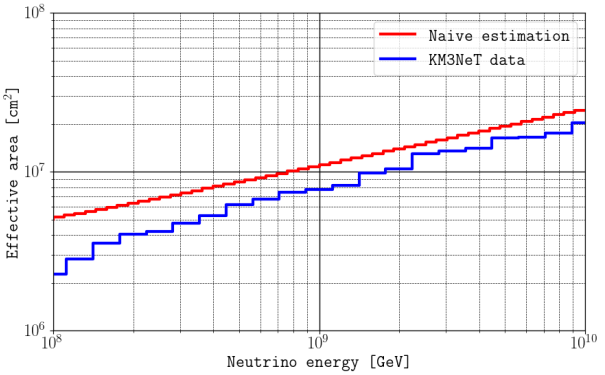

FIG. 5: KM3NeT effective area with respect to muon neutrinos. The red line represents a naive estimation, the blue line corresponds to the KM3NeT data [3].

We note a very good agreement with the real effective area, within a factor of 3. We overestimate the real data because of imperfect trigger and muon detection in the real world.

III. ISOTROPIC FLUX MODEL

The simplest neutrino flux model is isotropic with a customary E^{-2} spectrum. We estimate this flux based on the single event in KM3NeT via maximum likelihood. The number of expected events in the detector is

$$\bar{n} = \int_{E_{min}}^{E_{max}} \Phi \cdot E^{-2} \cdot A_{\text{eff}}(E) \cdot 4\pi \cdot T \cdot dE. \quad (3)$$

We then estimate the flux assuming Poisson statistics for the number of arrived events and get

$$\Phi_{\text{KM3NeT}} = 3.8^{+12.7}_{-3.2} \cdot 10^{-8} \text{ GeV cm}^{-2} \text{ s}^{-1} \text{ sr}^{-1}. \quad (4)$$

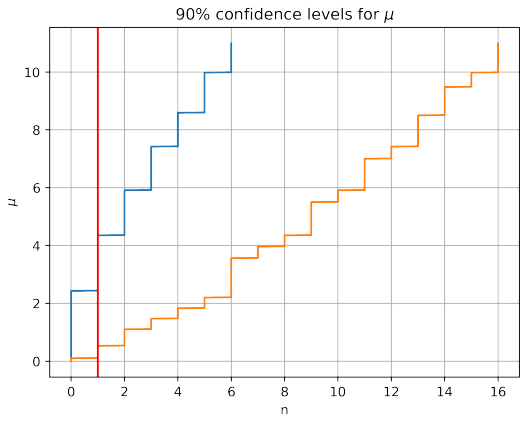

FIG. 6: Confidence Levels for different number of expected events μ vs. the number of events n.

The error is 90% CL following the Neumann error estimation method [4]. Fig. 6 and Fig. 7 show the confidence interval calculation. This error accounts for the fact that KM3NeT stopped the observation after just one event, and the estimator is unbiased.
This value agrees with the published flux of $\Phi = 5.8^{+10.1}_{-3.7} \cdot 10^{-8}$ GeV cm^{-2} s^{-1} sr^{-1}.

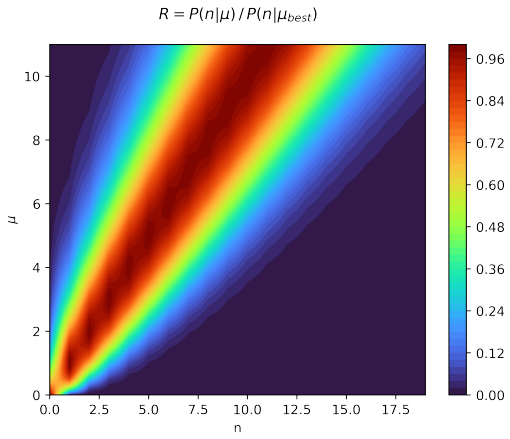

FIG. 7: R-parameter dependency on μ and n.

A. IceCube non-observation

If one accounts for the IceCube non-observation of any events in this energy range in the 9 years of operation, it is possible to perform a joint-fit estimation of the flux and the probability of such an outcome. One should get 1 event in the KM3Net and 0 events in IceCube. This joint fit results in an estimate of

$$\Phi_{\text{KM3+IC}} = 9.8^{+13.2}_{-4.5} \cdot 10^{-10} \text{ GeV cm}^{-2} \text{ s}^{-1} \text{ sr}^{-1}. \quad (5)$$

For this flux, the expected number of events in KM3NeT is $n_{\text{KM3}} = 0.025$ and in IceCube $n_{\text{IC}} = 0.97$. The probability of such an outcome is 0.009. This results in an upward fluctuation of approximately 2σ.
We also provide a Bayesian goodness-of-fit analysis. One wants to check that this power-law spectrum can describe both datasets. The tension is computed using the posterior predictive check approach. The joint probability is

$$p_{pcc} = \int\int P(\Phi, \gamma) \cdot \mathcal{L}_{IC} \cdot \mathcal{L}_{\text{KM3NeT}} \cdot d\Phi d\gamma \quad (6)$$

Here the prior distribution of variables is taken to be uniform. We than convert this probability to a z-score using the one-tail convention. This results in a tension of 2.4σ, which roughly corresponds to the frequentist approach.

B. Extension to lower energies

It is also possible to do a single power law fit to both the KM3NeT event and IceCube events in the PeV region (GOLD and BRONZE type events are used here). We treat the flux and spectral index as unknowns and estimate them in a similar way. This procedure yields a flux and spectral index of

$$\Phi_{\text{KM3+IC low}} = 2.1 \cdot 10^{-8}\ \text{GeV cm}^{-2}\ \text{s}^{-1}\ \text{sr}^{-1},\quad \gamma = -2.3, \quad (7)$$

but a probability of 0.001. This also coincides with the KM3NeT collaboration estimates within the errors [5].

IV. CONCLUSIONS

We estimate the detection probability and effective areas for KM3NeT and IceCube detectors. They are in good agreement with detailed calculation result provided by KM3NeT. We also provide estimates of neutrino flux with the assumption of an isotropic model. The flux obtained from only the KM3NeT event is unrealistically large. The estimates are also prone to big uncertanties, rooted in the fact that this is a single observation of a rare Poisson process. We provide a detailed error calculation that takes this into account.
The joint-fit for both IceCube and KM3NeT shows that this event (in this model) can be a fluctuation of 2σ significance. If lower energy IceCube events are taken into account, the probability of such an outcome remains very low, even with an arbitrary power law spectrum.
We believe that this analysis hints at a non-isotropic nature of this event. Possible explanations could be sources with flaring activity, like radio blazars or other similar objects.

[1] The KM3NeT Collaboration. "Observation of an ultra-high-energy cosmic neutrino with KM3NeT". In: *Nature* 638.8050 (Feb. 2025), pp. 376–382. ISSN: 1476-4687. DOI: 10.1038/s41586-024-08543-1. URL: https://doi.org/10.1038/s41586-024-08543-1.

[2] Víctor B. Valera, Mauricio Bustamante, and Christian Glaser. "The ultra-high-energy neutrino-nucleon cross section: measurement forecasts for an era of cosmic EeV-neutrino discovery". In: *Journal of High Energy Physics* 2022.6 (June 2022). ISSN: 1029-8479. DOI: 10.1007/jhep06(2022)105. URL: http://dx.doi.org/10.1007/JHEP06(2022)105.

[3] The KM3NeT Collaboration. *Data for the KM3-230213A high energy event observation*. 2025. URL: https://github.com/KM3NeT/KM3-230213A-data.

[4] S. et al. Navas. "Review of Particle Physics". In: *Phys. Rev. D* 110 (3 Aug. 2024), p. 030001. DOI: 10.1103/PhysRevD.110.030001. URL: https://link.aps.org/doi/10.1103/PhysRevD.110.030001.

[5] KM3NeT Collaboration. *The ultra-high-energy event KM3-230213A within the global neutrino landscape*. 2025. arXiv: 2502.08173 [astro-ph.HE]. URL: https://arxiv.org/abs/2502.08173.

TXS 0506–056 as a neutrino source. What can be derived from IceCube and Baikal-GVD observations?

Aleksandra Ivanova[1,2], Andrey Sheshukov[1], Anna Sirenko[1],
Pavel Volchugov[3], Yuliya Yablokova[1]

[1]*JINR,* [2]*ISU,* [3]*SINP MSU*

Project Author:
Grigory Rubtsov,
INR RAS

Scientific Advisor:
Andrey Sheshukov,
JINR

Abstract

The Baikal-GVD Collaboration reported [1] neutrino events near the position of the blazar TXS 0506–056, a location previously associated with a high-energy neutrino observed by IceCube [2]. This raises the question: is this spatial coincidence significant, and what does it reveal about the nature of the source? Our goal is to quantify the probability that both experiments would detect neutrino event near the same astrophysical source by chance, and explore what constraints such observations place on source models and detection systematics

I. SIGNAL MODEL DEFINITION

In general the model defines the differential neutrino flux from a given direction $\vec{\Omega}$

$$\Psi(\vec{\Omega}, t, E) \equiv \frac{d^3 N_\nu}{dt\, d\vec{\Omega}\, dE}\ [\mathrm{s}^{-1}\mathrm{srad}^{-1}\mathrm{m}^{-2}\mathrm{GeV}^{-1}] \tag{1}$$

A. Factorization

In our study we assume the energy, time and angular dependencies to be independent and factorizable

$$\Psi(\vec{\Omega}, t, E) = \Phi(\vec{\Omega}, t) \cdot g(E) = \\ = C \cdot f(t) \cdot F(\vec{\Omega}) \cdot g(E) \tag{2}$$

where C is an average integral rate $[\mathrm{s}^{-1}\mathrm{m}^{-2}]$:

$$\int_T dt \int d\vec{\Omega} \cdot \Phi(\vec{\Omega}, t) = CT \tag{3}$$

and other factors are normalized to one:

$$\int_T dt f(t) = T; \quad \int d\vec{\Omega}\ F(\vec{\Omega}) = 1 \tag{4}$$

In our study we consider the following source models:

1.1 Isotropic constant source $\bar{\Phi}$.

$$\bar{F}(\vec{\Omega}) = \frac{1}{4\pi}; \quad \bar{f}(t) = 1 \tag{5}$$

$$\bar{\Phi}(\vec{\Omega}, t|C) = \frac{C}{4\pi} \tag{6}$$

1.2 Point-like constant source $\bar{\Phi}^*$. The angular dependency is singular:

$$F^*(\vec{\Omega}) = \delta^2(\vec{\Omega} - \vec{\Omega}^*) \tag{7}$$

$$\bar{\Phi}(\vec{\Omega}, t|C, \vec{\Omega}) = C\delta^2(\vec{\Omega} - \vec{\Omega}^*) \tag{8}$$

1.3 Point-like flaring source $\tilde{\Phi}^*$. Intensity is assumed to be a periodic function. We can approximate it with a set of square pulses with period T and width τ:

$$\tilde{f}(t) = \sum_{n=0}^{\infty} \Theta(t - Tn) \cdot \Theta(Tn + \tau - t) \quad (9)$$

$$\tilde{\Phi}(\vec{\Omega}, t|C, \vec{\Omega}, T, \tau) = C \cdot \delta^2(\vec{\Omega} - \vec{\Omega}^*) \times \\ \times \sum_{n=0}^{\infty} \Theta(t - Tn)\, \Theta(Tn + \tau - t) \quad (10)$$

II. BACKGROUND

Astrophysical background. Parameterization from [3, eq. 4]

$$\Phi_A = \int_{E_{min}}^{\infty} dE\ \Phi_0 \cdot \left(\frac{E}{E_0}\right)^{-\gamma} \times \\ \times 10^{-18}\ \text{GeV}^{-1}\text{cm}^{-2}\text{s}^{-1}\text{sr}^{-1} = \\ = E_0\Phi_0 \cdot \left.\frac{(E/E_0)^{1-\gamma}}{1-\gamma}\right|_{E_{min}}^{\infty} = \\ = \frac{E_0\Phi_0}{(\gamma-1)(E_{min}/E_0)^{\gamma-1}} \quad (11)$$

Energy scale $E_0 = 100$ TeV and in our case the minimal energy $E_{min} = 200$ TeV.
Model parameters from [3] are shown on Tab. I

Obtained atmospheric neutrino spectrum at energies greater than 100 TeV is below astrophysical background. Therefore to simplify the background model we neglect it.

Baikal-GVD, based on [4]: Astrophysical neutrino event selection efficiencies were tested assuming a flux with equal numbers of neutrinos and anti-neutrinos, and with an equal neutrino flavor mixture at Earth:

$$(\nu_e : \nu_\mu : \nu_\tau) = 1 : 1 : 1.$$

The one flavor (1f) flux presented by **IceCube** was chosen as a baseline: MESE 2014.

Atmospheric neutrino.

IceCube
1. V.Agrawal *et al.* "Atmospheric neutrino flux above 1 GeV". Phys.Rev.D 53 (1996), pp.1314–1323. DOI:10.1103/PhysRevD.53.1314.
2. C.Mascaretti and F.Vissani. "On the relevance of prompt neutrinos for the interpretation of the IceCube signals". JCAP 2019.08 (2019), p.004. DOI:10.1088/1475-7516/2019/08/004.

Baikal-GVD
1. V.Allakhverdyan *et al.* arXiv:2211.09447. The conventional atmospheric neutrino flux from pion and kaon decays was modeled according to [L.V.Volkova, Sov.J. Nucl.Phys. 31, 784 (1980)]. Atmospheric prompt neutrinos were simulated according to the BERSS model [A.Bhattacharya *et al.*, JHEP 06, 110 (2015)].

2. Based on M.Kleimenov's Thesis Parametrization of atmospheric neutrino flux based on Vivek Agrawal *et al.* "Atmospheric neutrino flux above 1 GeV". Phys.Rev.D 53 (1996), pp.1314–1323. DOI:10.1103/PhysRevD.53.1314. Table of bartol flux points in file atmospheric_nu_flux.txt

TABLE I. IceCube and ANTARES Neutrino Analysis Results

Analysis	Energy Range	Φ_0	γ
HESE 2020	69.4 TeV–1.9 PeV	$2.12^{+0.49}_{-0.54}$	$2.87^{+0.20}_{-0.19}$
Cascades $\nu_e + \nu_\tau$ 2020	16 TeV–2.6 PeV	$1.66^{+0.25}_{-0.27}$	2.53 ± 0.07
MESE 2014	25 TeV–1.4 PeV	$2.06^{+0.4}_{-0.3}$	2.46 ± 0.12
Inelasticity 2018	3.5 TeV–2.6 PeV	$2.04^{+0.23}_{-0.21}$	2.62 ± 0.07
IceCube ν_μ 2016	194 TeV–7.8 PeV	$0.90^{+0.30}_{-0.27}$	2.13 ± 0.13
IceCube ν_μ 2019	40 TeV–3.5 PeV	$1.44^{+0.25}_{-0.24}$	$2.28^{+0.08}_{-0.09}$
ANTARES 2019	N/A	1.5 ± 1.0	2.3 ± 0.4

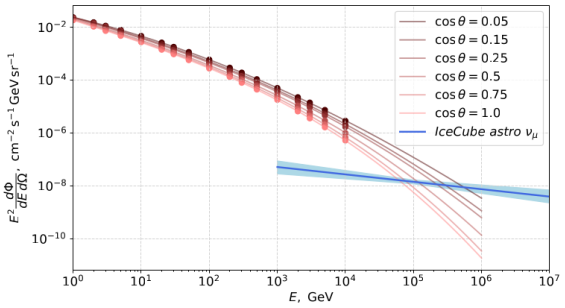

FIG. 1: Parameterization of the spectrum of atmospheric neutrinos as a function of the zenith angle θ (shades of red) and astrophysical muon neutrinos (blue) [M. Kleimenov, 2024].

III. DETECTOR MODEL

The detector model for the neutrino detection includes many complex features:

* interaction cross-section (E)
* Detection & selection efficiency vs. the neutrino angle and energy ($\vec{\Omega}, t, E$)
* detector exposure fraction for the given part of the sky ($\vec{\Omega}$)

This is estimated by the collaborations and as an **effective area** $A_{eff}(\vec{\Omega}, t, E)$.

Prediction of the observed event numbers. Observed event numbers N are given by

$$\int_{\Delta T} dt \int_{\Delta\Omega} d\vec{\Omega} \int_{\Delta E} dE\ A_{eff}(\vec{\Omega}, t, E)\Psi(\vec{\Omega}, t, E), \tag{12}$$

where ΔT, $\Delta\Omega$ and ΔE are the regions considered in the analysis.
In this analysis we just consider counting events $E_\nu > 200$ TeV, energy resolution (within reasonable limits) does not affect the result.
Angular region $\Delta\Omega$ is defined by the angular resolution. Time region is the total detector exposure. Using our factorization from signal models description, $N \propto$

$$\iiint_{\Delta(T;\Omega;E)} dt f(t)\, d\vec{\Omega}\, F(\vec{\Omega})\, dE\, g(E)\, A_{eff}(\vec{\Omega}, t, E) \tag{13}$$

TABLE II. Detector parameters from [1, Table 3].

Source spectrum	$A_{\text{eff}}^{\text{IceCube}}$	$A_{\text{eff}}^{\text{BGVD}}$
$E^{-2.0}$	$55.46\,\text{cm}^2$	$3.23\,\text{cm}^2$
$E^{-2.5}$	$31.27\,\text{cm}^2$	$2.9\,\text{cm}^2$

$$\bar{A}_{eff} = \\ = \int_{\Delta T} dt f(t) \int_{\Delta\Omega} d\vec{\Omega} \int_{\Delta E} dE\ g(E)\ A_{eff}(\vec{\Omega}, t, E) \tag{14}$$

So if we assume that $A_{eff}(\vec{\Omega}, t, E) \approx \bar{A}_{eff}$ in the regions of interest, we can use formula

$$N = \\ = \bar{A}_{eff} \cdot C \int_{\Delta T} dt f(t) \int_{\Delta\Omega} d\vec{\Omega} F(\vec{\Omega}) \int_{\Delta E} dE\ g(E) \tag{15}$$

Isotropic constant source (diffuse background):

$$\bar{N} = \bar{A}_{eff} \cdot C \cdot \Delta T \cdot \frac{\Delta\Omega}{4\pi} \tag{16}$$

Point source with constant rate:

$$\bar{N}^* = \bar{A}_{eff} \cdot C \cdot \Delta T \tag{17}$$

For this analysis we use the integrated $\bar{A}_{eff}$ for given point source, assuming the energy spectra and a flaring activity, as listed in Tab. II.
For the angular uncertainty we used $6.2°$ for cascades in BGVD, and $0.25°$ for track in IceCube, which leads to $\Delta\Omega_C = 1.49$ srad and $\Delta\Omega_T = 9.2 \cdot 10^-3$ srad, respectively.

IV. OBSERVATION SIGNIFICANCE

A. Hypotheses test

In order to test the significance of observation we need to consider the probability of our observation (1 track event in IceCube, and 1 cascade

event in Baikal-GVD) to be a random coincidence from background neutrino source.
We consider an isotropic background source with integral Φ_0.
For the significance we need to define the probability of:

- having at least 1 track in considered sky fraction S_{sky}
- which has at least 1 cascade within the cascade angular resolution Ω_C

B. Coincidence probability

Coincidence probability is composed of:

- Probability $P(n_t|N_T)$ to observe n_t tracks in the considered fraction of the sky S_{sky}: Poisson distribution with mean $N_T = A^T_{eff} \times \Phi_0 \times S_{sky}$
- Probability that at least one cascade is within an angular area of given n_t tracks: Poisson with mean $N_C = A^C_{eff} \times \Phi_0 \times n_t \times \Omega_C/4\pi$

Which leads to a final expression:

$$
\begin{aligned}
&P_{coinc}(\Phi_0, S_{sky}) = \\
&= \sum_{n_t=1}^{\infty} P(n_t|N_T) \cdot P(n_c > 0|N_C(n_t)) = \\
&= \sum_{n_t=1}^{\infty} P(n_t|\Phi_0 \times A^T_{eff} \times S_{sky}) \times \\
&\times \left(1 - \exp(\Phi_0 \times A^C_{eff} \times n_t \times \Omega_C/4\pi)\right)
\end{aligned} \tag{18}
$$

C. Sky regions of interest

We perform the study for several regions of interest:

- Full sky $S_{sky} = 1$, assuming a sensitivity to tracks and cascades in all 4π region. While technically incorrect, this gives us the most pessimistic estimation of the random coincidence probability.
- Half sky $S_{sky} = 1/2$, taking into account that IceCube considers only upward-going track events i.e. neutrinos from Northern hemisphere.
- Tracks pointing to one of the $N_{sources}$ within the Ω_T angular uncertainty: $S_{sky} = N_{sources} \times \Omega_T/4\pi$. We used $N_{sources} = 1694$ - a half of 3388 blazars used in [5].
- Finally we consider a probability to see the coincidence from a signle source (TXS 0506+056) direction $S_{sky} = \Omega_T/4\pi$.

D. Result

The resulting significance in σ vs. the integral background flux Φ_0 is show on Fig. 2
We compare this integral flux with the flux estimations, considered in [3], integrated for $E_\nu > 200\ TeV$, as described in sec. II.
The probability of having a track and cascade coincidence, associated with one of 1694 sources, generated by diffuse astrophysical neutrino background is rejected at $3.8 - 4.2\sigma$ level.

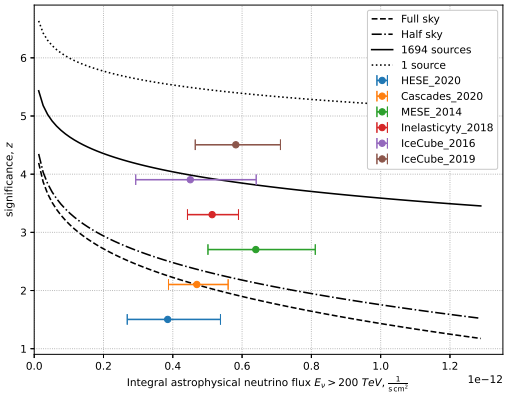

FIG. 2: significances for different models

V. SOURCE PARAMETERS ESTIMATION

We used Markov Chain Monte-Carlo approach to calculate the posterior distribution for the flux normalization parameter C.
In a simple approach without the account for systematics we used the values:

$$
\begin{aligned}
C &\sim \text{Uniform}(1e-17,\ 1e-11)\\
\text{expected events IceCube} &\sim \text{Poisson}(f(\text{C}))\\
\text{expected events Baikal} &\sim \text{Poisson}(f(\text{C}))\\
\text{C} &\sim \text{Uniform}(1e-17,\ 1e-11)\\
\text{bg\_flux\_IC} &\sim \text{TruncatedNormal}(4.64e-19,\ 3.21e-19,\ 0,\ inf)\\
\text{bg\_flux\_BGVD} &\sim \text{TruncatedNormal}(2.85e-16,\ 1.98e-16,\ 0,\ inf)\\
\text{eff\_area\_IceCube} &\sim \text{Normal}(3.13e+05,\ 3.13e+03)\\
\text{eff\_area\_Baikal} &\sim \text{Normal}(2.9e+04,\ 290)\\
\text{sum\_flux\_IC} &\sim \text{Deterministic}(f(\text{bg\_flux\_IC},\ \text{C}))\\
\text{sum\_flux\_BGVD} &\sim \text{Deterministic}(f(\text{bg\_flux\_BGVD},\ \text{C}))\\
\text{expected\_events\_IceCube} &\sim \text{Poisson}(f(\text{eff\_area\_IceCube},\ \text{bg\_flux\_IC},\ \text{C}))\\
\text{expected\_events\_Baikal} &\sim \text{Poisson}(f(\text{eff\_area\_Baikal},\ \text{bg\_flux\_BGVD},\ \text{C}))
\end{aligned}
$$

TABLE III. Constraints on the signal flux normalization

	16% percentile	**50% percentile**	**84% percentile**
without systematics, constant flux 5 year	2.5572×10^{-14}	4.8793×10^{-14}	8.4167×10^{-14}
with systematics, constant flux 5 year	2.5688×10^{-14}	4.9328×10^{-14}	8.6061×10^{-14}
without systematics, flare flux 2 year	6.3652×10^{-14}	1.2349×10^{-13}	2.1283×10^{-13}
with systematics, constant flux 2 year	6.3863×10^{-14}	1.2406×10^{-13}	2.1391×10^{-13}

VI. SUMMARY

Analysis and results

Coincidence probability

Calculated the likelihood of spatially coincident events arising from background:

- Poisson statistics for track (IceCube) and cascade (Baikal-GVD) events.
- Tested sky regions: full sky, northern hemisphere, regions around 1,694 blazars, and TXS 0506–056 specifically.
- The chance probability of a coincidence from background was rejected at 3.8–4.2σ when considering 1694 blazars, strengthening the case for TXS 0506–056 as a neutrino source.

Constraints on the neutrino source parameters

Key Implications

- The findings suggest that the observed neutrino events are unlikely to result from random background fluctuations.
- Systematic uncertainties (angular resolution, energy reconstruction) were shown to moderately affect significance but do not invalidate the conclusion.
- Both steady and flaring emission models are compatible with observations, though flaring scenarios require further temporal analysis.

[1] Baikal-GVD Collaboration et al. "High-energy neutrino-induced cascade from the direction of the flaring radio blazar TXS 0506+056 observed by Baikal-GVD in 2021". In: *Monthly Notices of the Royal Astronomical Society* 527.3 (Nov. 27, 2023), pp. 8784–8792. ISSN: 0035-8711, 1365-2966. DOI: 10.1093/mnras/stad3653. arXiv: 2210.01650[astro-ph]. URL: http://arxiv.org/abs/2210.01650 (visited on 04/05/2025).

[2] The IceCube et al. "Multi-messenger observations of a flaring blazar coincident with high-energy neutrino IceCube-170922A". In: *Science* 361.6398 (July 13, 2018), eaat1378. ISSN: 0036-8075, 1095-9203. DOI: 10.1126/science.aat1378. arXiv: 1807.08816[astro-

ph]. URL: http://arxiv.org/abs/1807.08816 (visited on 04/05/2025).

[3] Sergey Troitsky. "Constraints on the models of the origin of high-energy astrophysical neutrinos". In: *Physics-Uspekhi* 64.12 (Dec. 1, 2021), pp. 1261–1285. ISSN: 1063-7869, 1468-4780. DOI: 10.3367/UFNe.2021.09.03906210.3367/UFNr.2021.09.039062. arXiv: 2112.09611[astro-ph]. URL: http://arxiv.org/abs/2112.09611 (visited on 04/10/2025).

[4] Baikal Collaboration et al. "Diffuse neutrino flux measurements with the Baikal-GVD neutrino telescope". In: *Physical Review D* 107.4 (Feb. 21, 2023), p. 042005. ISSN: 2470-0010, 2470-0029. DOI: 10.1103/PhysRevD.107.042005. arXiv: 2211.09447[astro-ph]. URL: http://arxiv.org/abs/2211.09447 (visited on 04/10/2025).

[5] Alexander Plavin et al. "Observational Evidence for the Origin of High-energy Neutrinos in Parsec-scale Nuclei of Radio-bright Active Galaxies". In: *Astrophys. J.* 894.2 (2020), p. 101. DOI: 10.3847/1538-4357/ab86bd. arXiv: 2001.00930 [astro-ph.HE].

Muon and Electron Signatures in Super–Kamiokande and Sensitivity to Proton Decay

Angelina Chvirova[1], Daria Fedorova[1,2]
[1]*INR RAS,* [2]*MIPT*

Project Author:
Jianglai Liu,
TD Li Institute

Scientific Advisor:
Alexey Kuznetsov,
JINR

Abstract

Muons and electrons are both charged leptons but exhibit very different behavior in detectors due to their mass and interaction processes. Super–Kamiokande (SK), a large water Cherenkov detector, is used to detect neutrinos and search for rare processes like proton decay. This project investigates the interaction and detection characteristics of muons and electrons and evaluates the sensitivity of SK to proton decay.
Analyze and compare the energy deposition mechanisms of muons and electrons, estimate particle ranges, and determine the limits of full containment in SK. Evaluate its sensitivity to proton decay assuming optimal detection conditions.

I. ENERGY DEPOSITION DIFFERENCES

Electrons ($m_e c^2 = 0.511\,\text{MeV}/c^2$) and heavy charged particles (for example, muon $m_\mu c^2 = 105.658\,\text{MeV}/c^2$) are able to lose energy in matter through ionization, radiation (bremsstrahlung), and pair production.
In the region of low electron energies ($E < 10$ MeV), ionization processes of interaction with atomic electrons, including the ionization of atoms, provide the determining contribution to energy losses.
Specific ionization energy losses of electrons[1]:

$$\left(\frac{dE}{dx}\right)_{e\text{ ion}} = -\frac{2\pi}{\beta^2} n_e r_e^2 m_e c^2 \times \times \left[\ln\left(\frac{m_e c^2 T_e}{\bar{I}^2}\cdot\frac{\beta^2}{2(1-\beta^2)}\right) - \left(2\sqrt{1-\beta^2}-1+\beta^2\right)\ln 2 + 1 - \beta^2\right], \quad (1)$$

where m_e – mass of the electron; T_e – kinetic energy of the electron; $\beta = \frac{v}{c}$, v – speed of the particle, c – speed of light; $n_e = N_A\left(\frac{Z}{A}\right)\rho$ – electron density of the medium, N_A – Avogadro's number, Z – medium atomic number, A – medium atomic mass, ρ – medium density; $\bar{I}$ – mean ionization potential of the atoms in the medium: $\bar{I} = 13.5\,Z$ eV, $r_e = \frac{e^2}{m_e c^2} = 2.818 \cdot 10^{-13}$ cm – classical electron radius.
Hard collision (Moller scattering) is elastic scattering of an electron on an atomic electron. A charged particle (electron) transfers part of its energy to the atomic electron. As a result, the atomic electron is knocked out of the atom and becomes a δ -electron that is also able to produce ionization. This process occurs at $E < 10$ MeV.
For electrons, it is also significant that at energies of a few MeV, radiative losses become noticeable. At higher energies, radiation losses dominate over ionization losses ($E > 10$ MeV).
Specific radiative energy loss of electrons:

$$\left(\frac{dE}{dx}\right)_{e\text{ rad}} = -E_e \cdot \frac{1}{X_0}, \quad (2)$$

where E_e – energy of the electron; X_0 – radiation length of the material, a characteristic length over which an electron loses all but $1/e$

[1] All following formulas are taken from [1].

of its energy due to bremsstrahlung.
A high-energy electron in the field of the nucleus (or atomic electron) produces an electron-positron pair. Pair production becomes significant at $E > 10$ GeV and competes with bremsstrahlung at $E > 100$ GeV. Energy losses of electrons for pair production:

$$\left(\frac{dE}{dx}\right)_{\text{e pair}} = -\alpha r_e^2 \frac{Z^2}{A} E_e \rho \cdot \Phi(E, Z), \quad (3)$$

where α – fine structure constant; Z – medium atomic number; A – medium atomic mass; ρ – medium density; $\Phi(E, Z)$ – function that takes into account the kinematics of the process.
Muons are heavy charged particles. The ionization losses for them dominate in the whole energy range (especially at $E < 100$ GeV). Specific ionization energy losses of muons:

$$\left(\frac{dE}{dx}\right)_{\mu\text{ ion}} = -Kz^2 \times$$
$$\times \frac{Z}{A}\frac{1}{\beta^2}\left[\frac{1}{2}\ln\left(\frac{2m_e c^2 \beta^2 \gamma^2 T_{\max}}{\bar{I}^2}\right) - \beta^2 - \frac{\delta}{2}\right], \quad (4)$$

where K – simplifying constant, $K = 0.307\,\text{MeV} \cdot \text{cm}^2/\text{g}$; z – charge of the muon; γ – relativistic factor, $\gamma = \frac{E}{m_\mu c^2}$; T_{max} – maximum kinetic energy transfer in a single collision; δ – density correction.
Hard collision (Moller scattering) also occurs with a muon on an atomic electron, but it is negligible. The cross section of the process is inversely proportional to the muon mass. When a heavy particle scatters on a light particle, the momentum/energy transfer is small (as when a billiard ball hits a grain of sand).
The braking radiation for muons is negligible at $E < 100$ GeV (due to their mass as well). Specific radiative energy loss of muons (significant at $E > 1$TeV):

$$\left(\frac{dE}{dx}\right)_{\mu\text{ rad}} = -\left(\frac{m_e}{m_\mu}\right)^2 E_\mu \cdot \frac{1}{X_0}, \quad (5)$$

where E_μ – energy of the muon; X_0 – radiation length of the material, a characteristic length over which an electron loses all but $1/e$ of its energy due to bremsstrahlung.
A muon in the nucleus field emits a virtual photon, which transforms into an electron-positron pair, but this process is rare and only becomes important at ultra-relativistic energies($E > 1$ TeV), due to suppression in $\left(\frac{m_e}{m_\mu}\right)^2 \approx 10^{-4}$. Energy losses for pair birth:

$$\left(\frac{dE}{dx}\right)_{\mu\text{ pair}} = -\alpha r_e^2 \frac{Z^2}{A} E_\mu \rho \left(\frac{m_e}{m_\mu}\right)^2 \cdot \Phi(E, Z). \quad (6)$$

In brief:

- Ionization losses are the main loss mechanism for electrons at $E < 10$ MeV and dominate the entire energy range for muons (especially at $E < 100$ GeV). Electrons have a shorter range due to their mass and strong scattering, while muons have a longer range (≈ 200 times longer e at the same energy).

- Hard collision (Moller scattering) is critical for electrons at $E < 1$ MeV, forms δ-electrons, and is negligible for muons at $E < 1$ TeV. Moller scattering for muons at $E > 1$ TeV is formally possible, but still uncompetitive with radiative losses.

- Braking radiation (bremsstrahlung) is dominant for electrons at $E > 10$ MeV and negligible for muons at $E < 100$ GeV. Braking radiation becomes significant for muons at $E > 100$ GeV and dominates at $E > 1$ TeV.

- Pair production becomes significant for electrons at $E > 10$ GeV and competes with bremsstrahlung at $E > 100$ GeV. For muons, the process is suppressed and is only relevant at ultra-high energies $E > 1$ TeV.

  Super–Kamiokande is able to detect neutrinos in the energy range from 4.5 MeV to 1 TeV. As a result of quasi-elastic scattering of neutrinos through a charged current, negatively charged particles such as electrons and muons appear:

  $$\nu_e + n \to e^- + p,$$

  $$\nu_\mu + n \to \mu^- + p.$$

  The identification of events in the detector is based on the shape and size of the Cherenkov rings.

- For electrons produced by electron neutrinos, radiation losses and electromagnetic showers dominate, forming a fuzzy cone of Cherenkov light. At energies below $E < 100$ MeV, showers do not develop, so such rings are less fuzzy.

- Muons produced by the muon neutrino in the process of their passage through the detector form a clear cone of Cherenkov radiation due to the main process of ionization losses. Cherenkov light concentrates along the track. For muons with $E > 10$ GeV, radiation losses are possible, but they are rare in SK.

A comparison of the described Cherenkov rings is shown in Fig. 1.

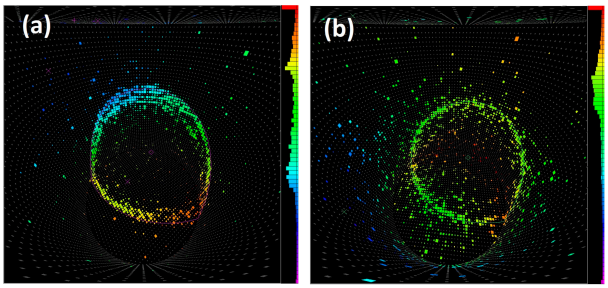

FIG. 1: Cherenkov rings detected by SK in 1998: (a) from muons with a momentum of 604 MeV, (b) from electrons with a momentum of 492 MeV. This figure of a simulation in the SK detector is a courtesy of the SK collaboration.

II. RANGE ESTIMATION IN MATTER

Electrons lose energy via radiation. The range R_e can be estimated as:

$$R_e \approx \frac{X_0}{\rho} \cdot \ln\left(\frac{E_e}{E_c}\right), \tag{7}$$

where X_0 – radiation length, ρ – medium density, E_c – critical energy, $E_c \approx 80$ MeV, E_e – initial energy.
Rough numerical estimations of R_e:

- Water:

$$R_e \approx \frac{36.1}{1} \cdot \ln(\frac{1000}{78}) \approx 90 \text{ cm},$$

- Lead:

$$R_e \approx \frac{6.4}{11.3} \cdot \ln(\frac{1000}{7.8}) \approx 2.7 \text{ cm}.$$

Muons lose energy via ionization. The range R_μ can be estimated as:

$$R_\mu \approx \frac{E_\mu}{\rho_w \left\langle \frac{dE}{dx} \right\rangle}, \tag{8}$$

where $\left\langle \frac{dE}{dx} \right\rangle$ – average energy loss per unit length (about 2 MeV $\cdot$ g^{-1}cm^2 for water and 1.3 MeV $\cdot$ g^{-1}cm^2 for lead). Rough numerical estimations of R_μ:

- Water:

$$R_\mu \approx \frac{1000}{1 \cdot 2} \approx 500 \text{ cm},$$

- Lead:

$$R_\mu \approx \frac{1000}{11.3 \cdot 1.3} \approx 70 \text{ cm}.$$

III. CONTAINMENT IN SK

The geometric size of the SK Inner Detector (ID) [2]:

- Total height: 36.2 m,
- Diameter: 33.8 m.

The fiducial volume (for neutrino interactions) is the virtual cylinder inscribed within the ID at a distance of 200 cm from its walls:

- Height (H_{fid}): $\sim$ 32 m,
- Diameter (D_{fid}): $\sim$ 30 m,

Maximum contained track length (diagonal to the cylinder):

$$L_{\text{max}} = \sqrt{H_{\text{fid}}^2 + D_{\text{fid}}^2} = \sqrt{32^2 + 30^2} \approx 44 \text{ m}.$$

Electrons lose energy via radiation. Their energy is calculated using equation (7):

$$(E_e)_{max} \approx E_c \cdot e^{\frac{L_{max} \cdot \rho_w}{X_0}} \approx 80 \cdot e^{\frac{44 \cdot 100}{36.1}} \approx \approx 2.6 \cdot 10^{52} \text{ GeV}.$$

Electrons with any energy will remain contained.

Muons lose energy via ionization (Bethe-Bloch). Their energy is calculated using equation (8):

$$(E_\mu)_{max} \approx L_{max} \cdot \rho_w \cdot 2 \text{ MeV} \cdot \text{g}^{-1}\text{cm}^2 \approx \approx 44 \cdot 100 \cdot 2 \approx 8.8 \text{ GeV}.$$

Multi-GeV muons will exit if they pass in the detector less than the specified length L_{max}. Muons with energy $E_\mu > 8.8$ GeV will escape the SK limit.

IV. PROTON DECAY SIGNAL

The expected signal for proton decay:

$$p \to e^+ + \pi^0.$$

This is one of the channels for proton decay searches in water Cherenkov detectors such as Super-Kamiokande. The positron produces a single Cherenkov ring (electron-like). The neutral pion decays almost immediately ($\tau \sim 10^{-17}$ s):

$$\pi^0 \to \gamma + \gamma.$$

Each photon from produces an electromagnetic shower (via pair conversion), resulting in two more electron-like rings. A maximum total of three Cherenkov rings are expected from proton decay.

A free (from H, are available in Super-K) proton is at rest, all of its energy is shared between the positron and neutral pion. They go in opposite directions to compensate for the momentum. Kinematic features of the event for a free proton:

$$\vec{p_p} = \vec{p_{\pi^0}} + \vec{p_{e^+}} = \vec{0} \Rightarrow p_{\pi^0} = p_{e^+}, \quad (9)$$

$$p = \sqrt{E^2 - m^2} = \sqrt{m^2 + 2mT + T^2 - m^2} = \\ = \sqrt{2mT + T^2}. \quad (10)$$

Combining equations (9) and (10), and energy conservation law:

$$\begin{cases} m_p = T_e + T_{\pi^0} + m_e + m_{\pi^0}, \\ 2m_e T_e + T_e^2 = 2m_{\pi^0} T_{\pi^0} + T_{\pi^0}^2. \end{cases} \quad (11)$$

From (11) can get that:

$$T_{e(\pi^0)} = \frac{1}{2m_p}(m_p - m_e - m_{\pi^0}) \times \\ \times (m_p - (+)m_e + (-)m_{\pi^0}). \quad (12)$$

Particle masses: m_p = 938 MeV, m_{π^0}= 135 MeV, $m_{e^+} \approx 0.5$ MeV (negligible). So far kinetic energy for the positron $T_e \approx 460$ MeV, for neutral pion $T_{\pi^0} = 340$ MeV. A positron with such energy will lose it via radiation. Thus, a ring from the positron will be electron-like.

Photons from a neutral pion usually have a small angle between them because of the limited momentum. So, the two rings can overlap or be very close. The type of rings from gammas will be electron-like.

The signature of a free proton decay will be characteristic rings on opposite sides of the detector (back-to-back). If we consider a proton inside the oxygen nucleus, decay products can undergo nuclear effects [3]. Due to nuclear effects, observable particles can differ from a "free proton" particles. For example, a neutral pion interaction inside a nucleus would result in positive pion production. This positive pion would give (depending on the energy) a a muon-like ring or no ring at all. Nuclear effects spoil the signal and make it inseparable from backgrounds.

Main Backgrounds:

- Atmospheric neutrino interactions through a charged-current:

$$\nu_e + n \to e^- + p,$$

$$\bar{\nu_e} + p \to e^+ + n.$$

- Interactions of muon neutrinos from the beam.
- Neutrino interactions through a neutral-current:

$$\nu + p \to \nu + p + \pi^0.$$

- Cosmic muons decays:

$$\mu^- \to e^- + \bar{\nu_e} + \nu_\mu,$$

$$\mu^+ \to e^+ + \nu_e + \bar{\nu_\mu}.$$

The following cuts can be used to suppress backgrounds:

- Interaction vertex inside Super-Kamiokande FV.
- No delayed signal (from charged pions decay).
- Total collected energy ≈ 940 MeV.
- No tagged neutron: to tag neutrons and thus differentiate the signal from some backgrounds' channels, Gd (0.01%) was added to Super-Kamiokande.
- Back-to-back topology for e-like rings.

V. PROTON LIFETIME SENSITIVITY

Proton Lifetime Lower Bound Estimation for Super-Kamiokande

Experimental parameters:

- Fiducial mass: $M_{\text{fid}} = 22.5\,\text{kt} = 2.25 \times 10^{10}\,\text{g}$ of water,
- Proton count per gram: $N_p/\text{gram} = 6.022 \times 10^{23} \cdot \frac{10}{18} \approx 3.35 \times 10^{23}$,
- Total protons: $N_p = 2.25 \cdot 10^{10} \times 3.35 \cdot 10^{23} \approx 7.5 \times 10^{33}$,

- Exposure time: $T = 10$ year $\approx 3.15 \times 10^8$ s.

Statistical limit calculation

For zero observed decays with perfect efficiency and no background, the 90% confidence level lower limit on the proton lifetime τ_p follows from Poisson statistics:

$$P(0) = e^{-\mu} \geq 0.1 \quad \Rightarrow \quad \mu \leq \ln(10) \approx 2.3026,$$

where μ is the expected number of decays:

$$\begin{aligned} \mu &= N_p - N_p(T) = \\ &= N_p - N_p \cdot \exp(-T/\tau_p) \approx \\ &\approx N_p \cdot (1 - (1 - T/\tau_p)) = N_p \cdot T/\tau_p, \end{aligned} \quad (13)$$

$$\mu = \frac{N_p \cdot T}{\tau_p}.$$

Combining these gives:

$$\begin{aligned} \tau_p &\geq \frac{N_p \cdot T}{\ln(10)} \approx 0.434 N_p T \geq \\ &\geq 7.5 \times 10^{33} \times 3.15 \times 10^8 \times 0.434 \geq \\ &\geq \boxed{1.03 \times 10^{42} \text{ s} \approx 3.26 \times 10^{34} \text{ years}}. \end{aligned}$$

Comparison with Actual Limits

- Current SK limit (2017) [4]: $\tau/B(p \to e^+\pi^0) > 2.4 \times 10^{34}$ year – obtained constraint ~ 1.5 times longer than published.

[1] S. Navas et al. "Review of particle physics". In: *Phys. Rev. D* 110.3 (2024), p. 030001. DOI: 10.1103/PhysRevD.110.030001.

[2] Y. Fukuda et al. "The Super-Kamiokande detector". In: *Nucl. Instrum. Meth. A* 501 (2003). Ed. by V. A. Ilyin, V. V. Korenkov, and D. Perret-Gallix, pp. 418–462. DOI: 10.1016/S0168-9002(03)00425-X.

[3] M. V. N. Murthy and K. V. L. Sarma. "Proton Decay Inside the Nucleus". In: *Phys. Rev. D* 29 (1984), pp. 1975–1984. DOI: 10.1103/PhysRevD.29.1975.

[4] K. Abe et al. "Search for proton decay via $p \to e^+\pi^0$ and $p \to \mu^+\pi^0$ in 0.31 megaton·years exposure of the Super-Kamiokande water Cherenkov detector". In: *Phys. Rev. D* 95.1 (2017), p. 012004. DOI: 10.1103/PhysRevD.95.012004. arXiv: 1610.03597 [hep-ex].

Production and Use of ^{18}F for Neutrino Detector Calibration

Truong Hoai Bao Phi[1], Anastasiia Kalitkina[1], Alim Kanshaov[2]
[1]*JINR,* [2]*KBSU*

Project Author:
Jianglai Liu,
TD Li Institute

Scientific Advisor:
Irina Perevalova,
ISU & JINR

Abstract

Prof. Jianglai Liu discussed that certain n-activated radionuclides are valuable for calibrating neutrino detectors. One such isotope is fluorine-18 (^{18}F), a e^+ emitter widely used in medical imaging and neutrino physics. In this project, you will design a method to produce ^{18}F using a compact n-generator, analyze its decay signature, and study its application in calibrating a liquid scintillator detector (LSD), like JUNO [1].

I. DESIGN OF THE ACTIVATION SETUP

Firstly, we need to figure out how to obtain a sample with ^{18}F from polytetrafluoroethylene (PTFE). PTFE is a synthetic fluoropolymer widely recognized for its exceptional chemical resistance, thermal stability, and low friction properties. Commercially known as Teflon, PTFE is a white, waxy solid at room temperature. PTFE consists of a carbon backbone fully substituted with fluorine atoms, giving it the formula $(C_2F_4)_n$. Therefore, PTFE is chemically pure and contains a high proportion of fluorine atoms, ensuring minimal contamination. In addition, PTFE is quite cheap and widely available and can be processed into various forms to suit experimental needs.
According to the task requirements, the production of ^{18}F for neutrino detector calibration will involve the irradiation of PTFE samples using a neutron generator. Neutron generators are compact devices that produce neutrons through nuclear fusion reactions, primarily using deuterium (D) and tritium (T). We have discussed two possible options.

1. Deuterium-Deuterium (D-D) generator:
   $^2\mathrm{H} + {}^2\mathrm{H} \rightarrow {}^3\mathrm{He} + n$, where $E_n \approx 2.5$ MeV
2. Deuterium-Tritium (D-T) generator:
   $^2\mathrm{H} + {}^3\mathrm{H} \rightarrow {}^4\mathrm{He} + n$, where $E_n \approx 14$ MeV

PTFE irradiation with fast neutrons is described by the nuclear reaction

$$^{19}\mathrm{F}(n, 2n)^{18}\mathrm{F}, \qquad (1)$$

which energy threshold is 10.4 MeV. Based on this fact, we can use only the D-T generator. The TANGRA facility at JINR [2] provides an example of such a generator. The core of TANGRA is a portable D-T neutron generator with a flux of up to 10^8 n/s. A schematic of this generator is shown in Fig. 1. It is worth noting that the neutron flux used in the following calculations is 10^6 $n/\mathrm{s}/\mathrm{cm}^2$, as specified in the task conditions.

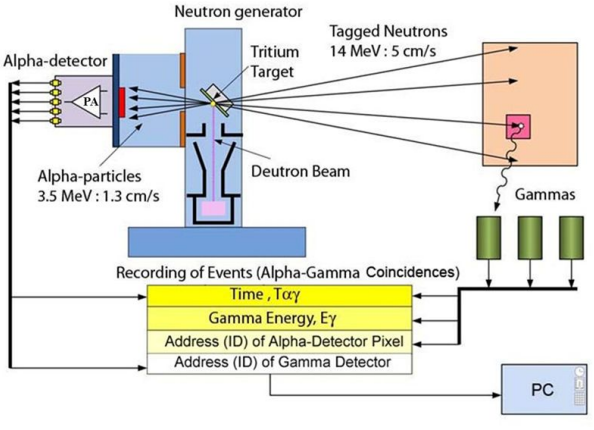

FIG. 1: Schematic diagram of the tagged neutron generator setup, illustrating the production of 14 MeV neutrons via the $^3\mathrm{H}(d, n)^4\mathrm{He}$ reaction.

The cross-section of reaction (1) depends on the neutron energy, as shown in Fig.2. According to this plot, if our hypothetical D-T generator pro-

duces neutrons with energy about 14 MeV, the reaction cross-section $\sigma \approx 0.05 \pm 0.01$ b.

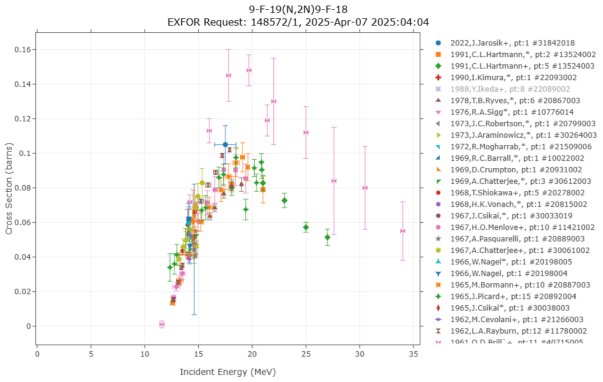

FIG. 2: Experimental cross-section data for the $^{19}\mathrm{F}(n, 2n)^{18}\mathrm{F}$ reaction as a function of incident neutron energy, compiled from the Experimental nuclear reaction data (EXFOR) database [3].

The activity of the irradiated sample increases during irradiation and approaches a saturation value when the production and decay rates become equal. It can be described by formula:

$$A(t) = \lambda N(t) = \phi\sigma N_0(1 - e^{-\lambda t}), \quad (2)$$

includes dependencies on the neutron flux ϕ, the cross section of the reaction σ, the number of target nuclei N_0, the decay constant λ, and the irradiation time t. The flux and the cross section have been defined above. The decay constant depends inversely on the half-life of an isotope:

$$\lambda = \frac{ln(2)}{T^{1/2}}, \quad (3)$$

for $^{18}\mathrm{F}$ $T^{1/2} \approx 110$ min. To determine the irradiation time, we have considered two options for the target mass, which are 5 g and 10 g of PTFE. As shown in Fig. 3, the time required to produce 100 Bq of $^{18}\mathrm{F}$ is approximately 3 minutes for a 5 g PTFE sample. This result is consistent with the estimate from [4], which reports a production time of less than 10 minutes for a cylindrical PTFE sample of comparable mass. The increase in irradiation time accounts for two key factors:

- Self-shielding effects within the PTFE sample, which reduce neutron flux penetration.

- The delay between the end of irradiation and the start of calibration, ensuring sufficient $^{18}\mathrm{F}$ accumulation for reliable measurements.

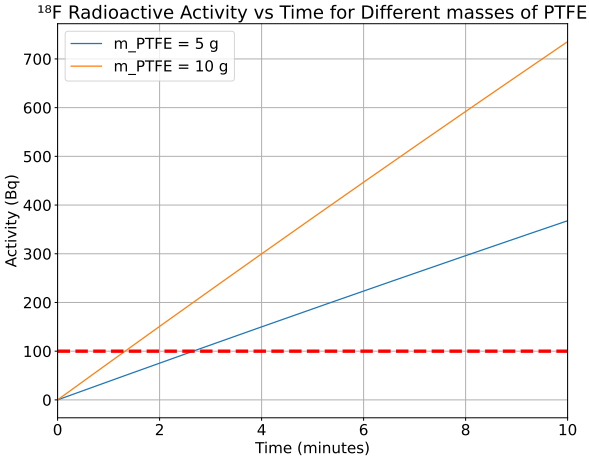

FIG. 3: Radioactive activity of $^{18}\mathrm{F}$ as a function of irradiation time for PTFE samples with masses of 5 g and 10 g. The red dashed line indicates the required activity of 100 Bq.

II. DECAY PROPERTIES

$^{18}\mathrm{F}$ is a key positron-emitting radioisotope. Positron emission accounts for 96.7% of decays, producing a positron and a neutrino while transforming into stable $^{18}\mathrm{O}$. The emitted positrons have a maximum energy of 635 keV and a continuous spectrum with a peak between 200 and 300 keV. In 3.3% of decays, electron capture occurs, directly yielding $^{18}\mathrm{O}$ without positron emission.
The endpoint of positron ionization is annihilation, producing two γ with energy 511 keV. Therefore, $^{18}\mathrm{F}$ is a source of γ with energy that mimics the prompt signal of inverse β-decay (IBD) events. Furthermore, short half-life allows repeating calibration without long-term contamination. As shown in section I, radioactive sample with $^{18}\mathrm{F}$ can be easily generated before each deployment at the large LSD site along expected operational life of the experiment.

III. DETECTOR RESPONSE MODELING

Assuming the irradiated PTFE is sealed in a stainless-steel capsule and placed in the center of a large LSD. Firstly, it prevents contamination to LSD. Secondly, the capsule shields positrons, so positron annihilation occurs only in the PTFE sample or in the capsule. Consequently, scintillation light is produced by γ-pairs. As shown in Fig. 4, the detector response forms from:

- Compton Continuum (0 - 340 keV): Partial energy deposition from scattered gammas, with a sharp edge at 340 keV (Compton edge).

- A gaussian-like peak at 511 keV when the gamma deposits all its energy, assuming a signal from a γ-pair is read out as two single events.

- A gaussian-like peak at 1 MeV when the γ-pair deposits all its energy.

If the stainless-steel capsule is sufficiently thick, it will fully contain the positrons, preventing them from reaching the detector and inducing quenching effects. Under these conditions, the proposed calibration method remains reliable, as the positron kinetic energy does not contribute to the measured light yield. Without taking into account the detection efficiency and other effects, the number of photoelectrons (PE) collected from positron annihilation can be calculated by knowing the photon yield. The project condition suggests 1600 PE per MeV. Working only with energy integrated from whole detector, the 2γ-peak around 1 MeV can be described by Poission distribution (see Fig.5):

$$P(\mu, n) = \frac{\mu^n}{n!} e^{-\mu}, \tag{4}$$

where mean value $\mu = 2 \cdot 511[\text{keV}] \cdot 1600[\text{PE}/1\ \text{MeV}]$, and n is the number of ^{18}F decays.

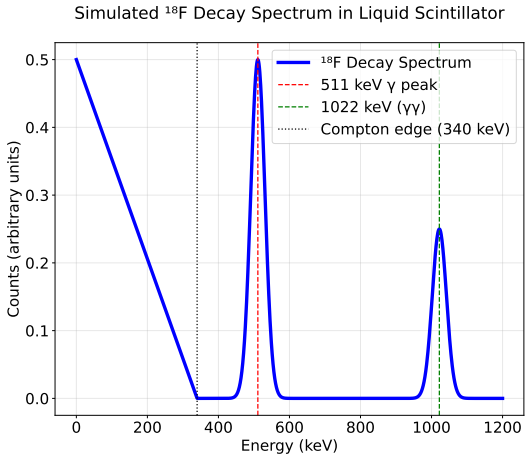

FIG. 4: Simulated ^{18}F decay spectrum, assuming 50% of the detection efficiency.

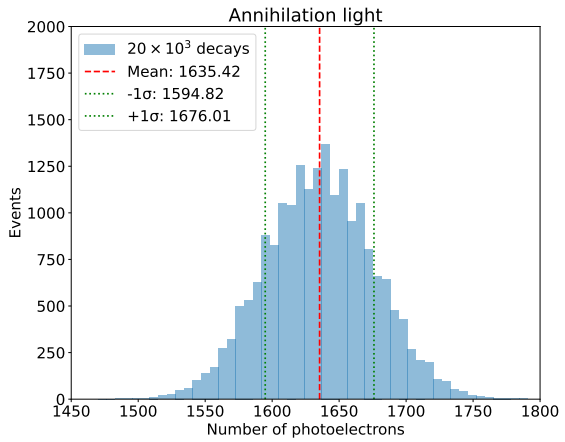

FIG. 5: Poission distribution of the number of PE detected for positron annihilation from 20,000 ^{18}F decays.

IV. CALIBRATION PRECISION

We can estimate the energy resolution and calibration precision of our method using Poisson distribution variables. An uncertainty in the peak position is equal to $\sqrt{\mu/n}$, while an uncertainty in the distribution width is $\sqrt{2\mu^2/n}$. Suppose that the ideal precision for both energy peak reconstruction and width is when the relative uncertainty is less than 1%. Fig. 6 and Fig. 7 show the number of decays, which is enough to achieve this uncertainty. Namely, it is more than 6 events for the peak position, and more than 20,000 events for the peak width.

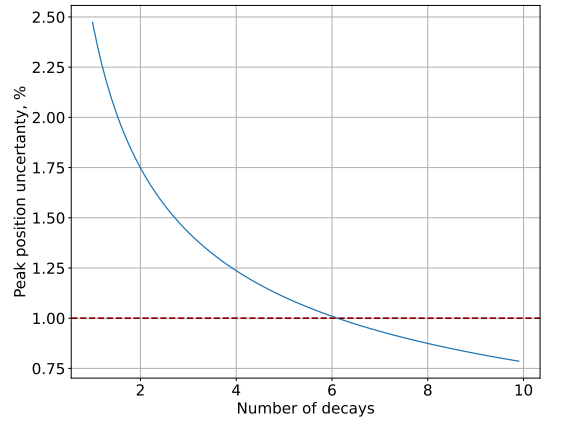

FIG. 6: Relative uncertainty in the peak position. The red dashed line indicates desired 1% uncertainty.

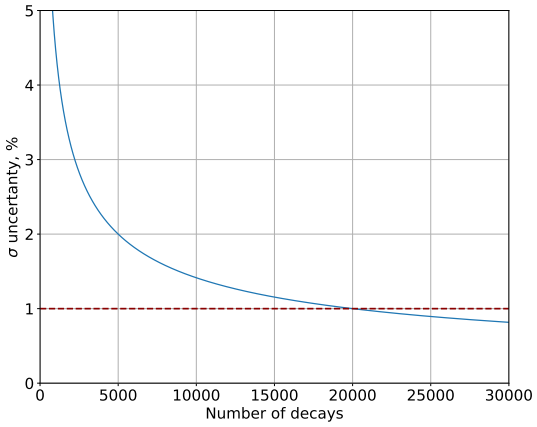

FIG. 7: Width as a function of the number of decays. The red dashed line indicates desired 1% uncertainty.

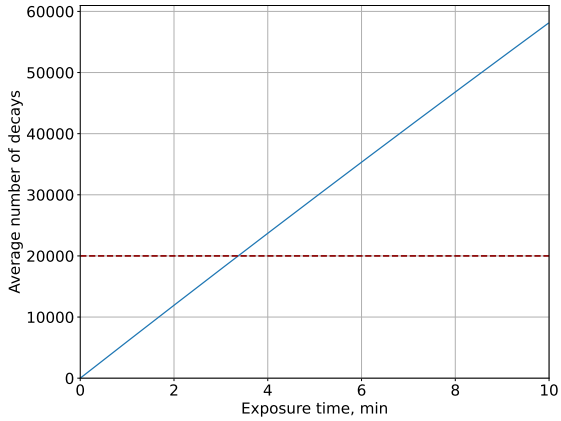

FIG. 8: The average number of ^{18}F decays as a function of time. The red dashed line indicates the desired number for precise calibration.

Estimates of the time the irradiated sample will be in the LSD are shown in Fig.8. As the initial activity of ^{18}F, $A_0 = 100$ Bq, decreases by law:

$$A(t) = A_0 e^{-\lambda t}, \tag{5}$$

with t being the post-irradiation time, the average number of decays becomes greater than 20,000 in 4 minutes.

V. CONCLUSION

^{18}F provides a viable source of positrons for calibrating large liquid scintillator detectors. Using a stainless-steel capsule ensures that only γ from positron annihilation deposit energy and mimic the prompt signal of IBD. Irradiating 5 g of PTFE with fast neutrons for approximately 5 minutes produces sufficient ^{18}F, and a 4-minute exposure within the detector achieves a calibration precision with less than 1% uncertainty in both the peak position and width. All of our calculations can be found at [5].

We acknowledge D. Dolzhikov, D. Ilyushkin, I. Perevalova, N. Anfimov for insightful discussions and support throughout this project.

[1] Fengpeng An et al. "Neutrino Physics with JUNO". In: *J. Phys. G* 43.3 (2016), p. 030401. DOI: 10.1088/0954-3899/43/3/030401. arXiv: 1507.05613 [physics.ins-det].

[2] I. N. Ruskov et al. "TANGRA-Setup for the Investigation of Nuclear Fission Induced by 14.1 MeV Neutrons". In: *Phys. Procedia* 64 (2015). Ed. by Franz-Josef Hambsch and Nicolae Carjan, pp. 163–170. DOI: 10.1016/j.phpro.2015.04.022.

[3] International Atomic Energy Agency. *Nuclear Data Services*. 2025. URL: https://www-nds.iaea.org.

[4] Akira Takenaka et al. "Customized calibration sources in the JUNO experiment". In: *JINST* 19.12 (2024), P12019. DOI: 10.1088/1748-0221/19/12/P12019. arXiv: 2410.01571 [physics.ins-det].

[5] A. Kalitkina and H. B. P. Truong. *Project calculations in Google Colab*. https://colab.research.google.com/p5.ipyhb. 2025.

Solar Neutrinos, Tritium Background, and Dark Matter in XENON1T

Olesia Geitota[1], Olga Lychagina[1], Alina Vishneva[1]
[1]*JINR*

Project Author:
Jianglai Liu,
TD Li Institute

Scientific Advisor:
Oleg Samoylov,
JINR

Abstract

The XENON1T experiment is a liquid xenon detector designed primarily for dark matter (DM) searches, but it is also sensitive to neutrino interactions and low-energy backgrounds. In 2020, an excess of low-energy electron recoil events was reported, leading to discussions about possible new physics or background explanations. This project explores solar neutrino interactions, background estimation, and expected DM signals. Estimate the number of expected neutrino and dark matter events in XENON1T, analyze the low-energy excess, and determine if it could be explained by a small amount of tritium contamination.

I. INTRODUCTION

The XENON1T experiment is a liquid xenon dual-phase time-projection chamber located in Laboratori Nazionali del Gran Sasso. It is primarily designed for the search of the so-called WIMPS (weakly interacting massive particles) — one of the most popular dark matter candidates. WIMPs are detected via the coherent elastic scattering on nuclei (CEνNS) but the experiment is also capable of detecting particles via the elastic scattering on electrons. It is also expected to be sensitive to solar neutrinos from the ^{8}B reaction via CEνNS on Xe nuclei. In 2020, the collaboration published their electron recoil spectrum featuring an excess of events in the 1–7 keV region [1].

II. OBJECTIVES

Properties:

- Detector mass: 1.04 ton
- Exposure time: 0.62 year
- Dark matter density: 0.3 GeV/cm^3
- Dark matter velocity: 220 km/s

Tasks:

1. Look up the flux and energy spectrum of ^{8}B solar neutrinos. Define the relevant energy range for elastic scattering with electrons and Xe nuclei.
2. Estimate the number of events due to $\nu-$e and ν-Xe coherent scattering.
3. Plot the differential energy spectra for both electron and nuclear recoils from solar neutrinos. Discuss the spectral shape and relevant features (e.g., recoil energy range, endpoint).
4. Use the XENON1T data (electron recoil spectrum) showing a slight excess at low energies. Assuming it is due to ^{3}H ($\tau_{1/2}$ = 13.2 years, Q = 18 keV), estimate total number of ^{3}H atoms in the detector.
5. For DM of mass 100 GeV/c^2, and cross section 10^{-42} cm^2, assuming a standard local DM density and velocity, estimate the expected number of DM-Xe scattering events.

III. SENSITIVITY TO ^{8}B SOLAR NEUTRINOS

Coherent elastic scattering of solar neutrinos from the ^{8}B reaction is a possible source of irreducible background for dark matter detectors. Among the other neutrino sources it is the closest one to the sensitivity range of modern DM experiments.
The energy spectrum of the ^{8}B neutrinos is available at [2].
As neutrinos are practically massless compared to electrons and nuclei, their elastic scattering process is compton-like with the maximal recoil energy

$$T_{\max}(E_\nu) = \frac{1}{1+\frac{M}{2E_\nu}}, \quad (1)$$

where M is the mass of the electron/nucleus and E_ν is the neutrino energy. As the endpoint of the ^{8}B neutrino spectra is 16.56 MeV, the recoil spectrum endpoint is 16.31 MeV for electrons and 4.49 keV for nuclei, respectively.

A. Electron Recoil

The differential cross section of the $\nu - e$ elastic scattering is:

$$\frac{d\sigma(E_\nu,T)}{dT} = \frac{2}{\pi}G_F^2 m_e \times \\ \times \left[g_L^2 + g_R^2\left(1-\frac{T}{E_\nu}\right) - g_L g_R m_e \frac{T}{E_\nu^2}\right], \quad (2)$$

where G_F is the Fermi constant, m_e is the electron mass, g_L and g_R are coupling constants:

$$g_L = \begin{cases} \frac{1}{2}+\sin^2(\theta_W) & \text{for } \nu_e \\ -\frac{1}{2}+\sin^2(\theta_W) & \text{for } \nu_\mu \text{ and } \nu_\tau \end{cases} \quad (3)$$

$$g_R = \sin^2(\theta_W), \quad (4)$$

and θ_W is the Weinberg angle.
Solar neutrinos are emitted as electron neutrinos but experience neutrino oscillations on their way to the detector and thus are detected as a mixture of flavors. Moreover, they experience the matter effect (Mikheyev–Smirnov–Wolfenstein (MSW) effect) while propagating in the Sun, so the survival probability of electron neutrinos gains energy dependence. We considered the MSW-LMA solution [3] for the survival probability of solar neutrinos and applied it to our estimation of the event rate. As the cross section of non-electron neutrinos is smaller than that of ν_e, we expect less events with respect to the non-oscillated signal model. The rate of neutrino interactions is then calculated as follows:

$$R = N_e \Phi_\nu \int dE_\nu \frac{d\lambda_\nu}{dE_\nu} \int_0^{T_{\max}} \left[\frac{d\sigma_e(E_\nu,T)}{dT}P_{ee}(E_\nu) + \right. \\ \left. \frac{d\sigma_{\nu,\tau}(E_\nu,T)}{dT}(1-P_{ee}(E_\nu))\right] dT, \quad (5)$$

where $N_e = 2.58 \cdot 10^{29}$ is the total number of electrons in the detector, Φ_ν is the total neutrino flux, $\frac{d\lambda_\nu}{dE_\nu}$ is the differential neutrino spectrum, P_{ee} is the survival probability of electron neutrinos.
The electron recoil sprectum can be calculated from equation (5) if we integrate only over E_ν. The comparison of the initial neutrino spectrum and the electron recoil spectra with and without neutrino oscillations is shown in Fig. 1.

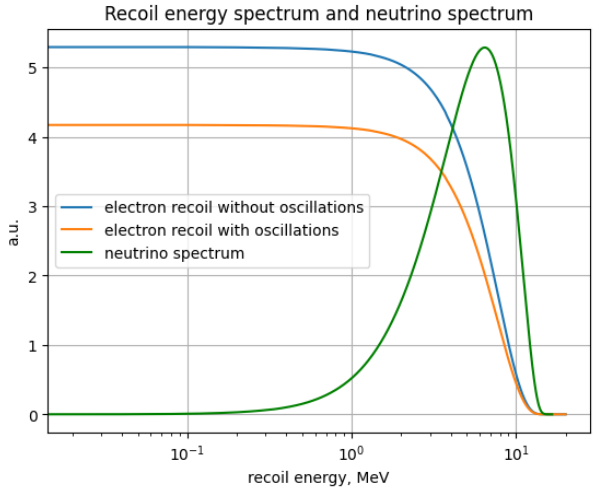

FIG. 1: Energy spectrum of ^8B solar neutrinos and electron recoil spectra with and without oscillations.

Integrating equation (5), taking into account the exposure time and assuming zero detection threshold, we get the next estimation for the number of electron recoils due to solar neutrinos: 0.94 ± 0.11 events in the non-oscillation case and 0.74 ± 0.09 events in the case of MSW-LMA neutrino mixing. In this estimation we considered the ^{8}B flux predicted by the Standard Solar Model with high metallicity (GS98) $\Phi_\nu = 5.46(1 \pm 0.12) \times 10^6$ cm^{-2}s^{-1} [4].

B. Nuclear recoil

The differential cross section of coherent elastic neutrino-nucleon scattering is [5]:

$$\frac{d\sigma(E_\nu,T)}{T} = \frac{G_F^2 M}{2\pi} Q_W^2 F^2(Q)\left(2 - \frac{MT}{E_\nu^2}\right), \quad (6)$$

where M is the nuclear mass, $Q_W = N - (1 - 4\sin^2\theta_W)Z$ is the weak nuclear charge, N and Z are the numbers of neutrons and protons in the nucleus, respectively, $F(Q)$ is the nuclear form factor as a function of the momentum transfer Q. In this estimation we consider full coherence and $F(Q) = 1$.
Coherent neutrino-nucleus scattering is a flavor-blind process, and equation (5) is reduced to

$$R = N_{\mathrm{Xe}}\Phi_\nu \int dE_\nu \frac{d\lambda_\nu}{dE_\nu} \int_0^{T_{\max}} \frac{d\sigma(E_\nu, T)}{dT} dT, \tag{7}$$

where $N_{\mathrm{Xe}} = 4.78 \cdot 10^{27}$ is the number of nuclei in the detector. Given the $^{131}_{54}$Xe properties, the total number of nuclear recoil events during the exposure time is 132.01 ± 16.14 under the assumption of zero detection threshold. The recoil spectrum is much less energetic with respect to the electron recoil (see Fig. 2), so in a real case the event rate would be suppressed due to the trigger efficiency of the detector at low energies.

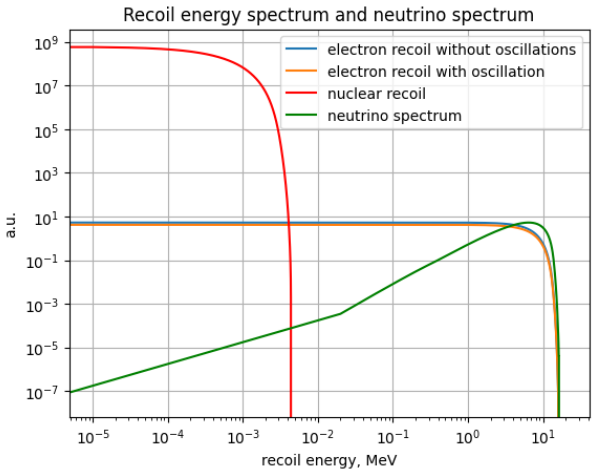

FIG. 2: Comparison of electron and nuclear recoil spectra for the same exposure. Normalization of the initial neutrino spectra is arbitrary.

TABLE V. Expected events in 1.04 ton × 0.62 yr exposure

^{8}B recoil type	Number of events
ER (non-ocs)	0.94 ± 0.11
ER (MSV-LMA)	0.74 ± 0.09
NR	132.01 ± 16.14

IV. LOW-ENERGY EVENT EXCESS AND THE TRITIUM BACKGROUND

A. Fit of the electron recoil spectrum

To study the tritium background hypothesis as a possible explanation of the low-energy excess in the electron recoil spectrum we performed a binned likelihood fit of the data spectrum with the sum of the standard background $f_B(T)$ and the tritium β-decay spectrum $f_{\mathrm{Tr}}(T)$:

$$f(T) = R_B \cdot f_B(T) + R_{\mathrm{Tr}} \cdot f_{\mathrm{Tr}}(T), \tag{8}$$

where event rates R_B and R_{Tr} are free parameters. The rate of tritium events from the fit is 158.38 ± 51.98 events/t/y, or 102.13 ± 33.52 events during the exposure time. The fit example is shown in Fig. 3.

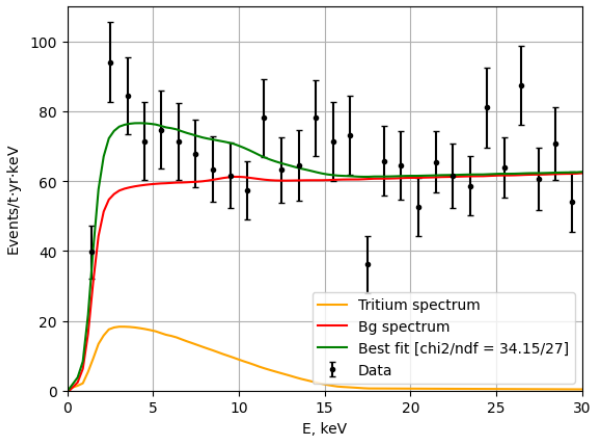

FIG. 3: Fit example. Resulting χ^2 value corresponds to p-value=0.16.

B. Number of tritium atoms in the detector

From the number of decays during the exposure time T_{exp} one can obtain the total number of tritium atoms in the detector. For isotopes with mean lifetime τ it reads

$$N_{\mathrm{total}} = \frac{N_{\mathrm{decays}}}{1 - \exp^{(-T_{\mathrm{exp}}/\tau)}} \tag{9}$$

For the mean lifetime of tritium $\tau = -\log(2) \cdot \tau_{1/2} = 17.75$ years, the total number of tritium atoms from the fit is 2974.31 ± 976.12.

V. DARK MATTER SEARCH

Dark matter flux can be expressed in terms of the standard dark matter properties as:

$$\Phi_{\mathrm{DM}} = n_{\mathrm{DM}} \cdot v_{\mathrm{DM}} = \frac{\rho_{\mathrm{DM}}}{M} \cdot v_{\mathrm{DM}}, \tag{10}$$

where ρ_{DM} and v_{DM} are the standard energy density and velocity of DM particles and M is the WIMP mass. WIMP interaction rate is then

$$R_{\text{DM}} = N_{\text{Xe}} \cdot \Phi_{\text{DM}} \cdot \sigma \qquad (11)$$

For DM of mass 100 GeV/c^2, and cross section 10^{-42} cm^2, one can get the rate of 0.01 event per year or 0.006 events during the exposure time.

VI. SUMMARY

As a result of the project, the following results were obtained:

- The data for the energy spectrum and flux of ^{8}B solar neutrinos were established. The relevant energy rages for or elastic scattering with electrons and Xe nuclei are $E_{ER} \in [0, 16.31]$ MeV and $E_{NR} \in [0, 4.49]$ keV respectively.
- The number of events due to ν-e and ν-Xe coherent scatterings were calculated. For ν-e scattering neutrino oscillations were been taking in account: $N_{ER}^{\text{non-ocs}} = 0.94 \pm 0.11$ and $N_{ER}^{\text{MSV-LMA}} = 0.74 \pm 0.09$. For nuclear recoils $N_{NR} = 132.01 \pm 16.14$.
- The differential energy specutra for both electron and nuclear recoils from solar neutrinos were plotted (Fig. 1, Fig. 2).
- The fits to XENON1T data under hypothesis of tritium nature of excess was produsedd. The rate of tritium events from the fit is 102.13 ± 33.52 events during the exposure time. The $\chi^2/ndf = 34.15/27$ means that assumption that exceed is due to ^{3}H is too approximate.
- for DM mass 100 GeV/c^2, andcross section 10^{-42} cm^2, assuming a standart local DM density and velocity (ρ_{DM} =0.3 GeV/c^2, v_{DM}=220 km/s), the expected number of DM-Xe scattering events were estimated: 0.006 events during the exposure time.

[1] E. Aprile et al. “Excess electronic recoil events in XENON1T”. In: *Phys. Rev. D* 102.7 (2020), p. 072004. DOI: 10.1103/PhysRevD.102.072004. arXiv: 2006.09721 [hep-ex].

[2] URL: https://www.sns.ias.edu/~jnb/SNdata/b8spectrum.html.

[3] P. C. de Holanda, Wei Liao, and A. Yu. Smirnov. “Toward precision measurements in solar neutrinos”. In: *Nucl. Phys. B* 702 (2004), pp. 307–332. DOI: 10.1016/j.nuclphysb.2004.09.027. arXiv: hep-ph/0404042.

[4] Núria Vinyoles et al. “A new Generation of Standard Solar Models”. In: *Astrophys. J.* 835.2 (2017), p. 202. DOI: 10.3847/1538-4357/835/2/202. arXiv: 1611.09867 [astro-ph.SR].

[5] Daniel Z. Freedman. “Coherent Neutrino Nucleus Scattering as a Probe of the Weak Neutral Current”. In: *Phys. Rev. D* 9 (1974), pp. 1389–1392. DOI: 10.1103/PhysRevD.9.1389.

Lunar-Based Ultimate Neutrino Telescope

Daniil Davydov[1,2], Vitaliy Dronik[3], Vladislav Filippov[3], Viktor Romanenko[2]
[1]*MSU,* [2]*INR RAS,* [3]*JINR,*

Project Author:
Dmitri Naumov,
JINR

Scientific Advisor:
Alexander Libanov,
INR RAS

Abstract

Imagine the next generation of neutrino astronomy, unconstrained by Earth limitations. The Moon offers a stable, low-background, seismically quiet, and atmosphere-free environment ideal for deploying a revolutionary neutrino telescope. This project explores the conceptual design of a Moon-based detector optimized for detecting ultra-high-energy astrophysical neutrinos.
Propose a realistic design of a large-scale neutrino detector on the Moon. Engineer the detection concept, estimate performance, and formulate a scientific case for funding a space-based mission to observe the most energetic neutrinos in the Universe.

I. INTRODUCTION

In this paper, we consider an acoustic method for detecting ulta-high-energy neutrinos on the Moon. We propose possible applications of acoustic detection, describe the optimal geometry and location of the detector system, and present a possible project deployment plan with a preliminary budget.
Observations made in recent years by experiments such as Auger and Telescope Array have confirmed the existence of cosmic accelerators capable of emitting charged particles with energies up to 100 EeV. The interaction of these highly energetic cosmic rays with gas or low-energy photons surrounding astrophysical sources or present in the intergalactic medium guarantees the emission of ultra-high-energy neutrinos. Ultra-high-energy neutrinos have great cosmological significance and may reveal new physics beyond the standard models. However, since the neutrino flux decreases with increasing energy, an observatory larger than one cubic kilometer will be required to detect them. Since a number of problems arise to register high-energy neutrinos on Earth, we propose to place a neutrino observatory on the surface of the Moon.

II. DETECTION METHOD

The acoustic neutrino detection technique is a promising approach for future large-scale detectors with the aim of measuring the small expected flux of cosmogenic neutrinos at energies exceeding 100 PeV. The technique is based on the thermo-acoustic model, which implies that the energy deposition by a particle cascade—resulting from a neutrino interaction in a medium with suitable thermal and acoustic properties—leads to a local heating and a subsequent characteristic pressure pulse that propagates in the surrounding medium [1].
A thermo-acoustic wave, generated by heating a suitable medium, can be described by the pressure difference p' between the ambient pressure p and the equilibrium pressure p_0, yielding the relation [2]:

$$\nabla^2 p' - \frac{1}{c_s^2}\frac{\partial^2 p'}{\partial t^2} = \frac{\partial^2 \epsilon}{\partial t^2}, \qquad (1)$$

where c_s is the adiabatic sound velocity and ϵ is the energy deposition density. This formulation assumes an isotropic energy deposition without momentum transfer to the medium. The general solution to this equation for the pressure difference measured at time t and position r is the

Kirchhoff integral [3]:

$$p'(\mathbf{r},t) = \frac{1}{4\pi}\frac{\alpha}{c_p}\int_V \frac{dV'}{|\mathbf{r}-\mathbf{r'}|}\frac{\partial^2}{\partial t^2}\epsilon\left(\mathbf{r'}, t - \frac{|\mathbf{r}-\mathbf{r'}|}{c_s}\right). \quad (2)$$

The maximal amplitude of the produced wave is in a direction orthogonal (incidence angle $= 90°$) to the axis of the cylinder. This is depicted in Fig. 1. In axial direction ($= 0°$) of the cylindrical volume only small signal amplitudes will be emitted. The expected frequency of the P wave is in the range between 10 to 60 kHz.

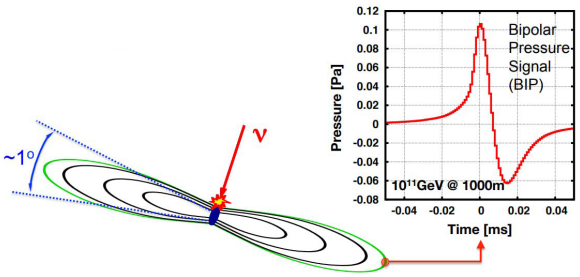

FIG. 1: Diagram of acoustic wave propagation in a medium and amplitude plot respectively.

Some of the reasons why the search for acoustic fingerprints of EeV neutrinos in bedrock has never been proposed could have been the lack of suitable infrastructures and concerns about the lack of uniformity of the geological formations. Also, the potential costs of producing a network of deep deposition holes in granite bedrock, covering an area of several square-kilometers, appears to be beyond practical consideration.
A concern is non-uniformity of the rock and the effect of cracks and layer boundaries on the signal propagation and attenuation. The possible fault lines will certainly degrade the acoustic properties. Another major concern is the significant background on Earth, which consists of:

- atmospheric neutrino background;
- natural and anthropogenic acoustic background.

The solution to these problems could be in placing the observatory on the Moon, which features some unique advantages:

- Atmospheric Interference. Earth's atmosphere absorbs EeV neutrinos, while moon, having no atmosphere allows direct detection. Zero atmospheric neutrino background (vs. 10^6 cm^{-2} s^{-1} on Earth);
- Ultra-Low Noise Environment. Seismic activity is $\sim 10^7$ weaker than Earth's and features no anthropogenic noise.

III. OPTIMAL LOCATION AND GEOMETRY OF THE DETECTOR

For a neutrino telescope, the ideal location on the Moon would be a place with the maximum thickness of lunar regolith (the material that absorbs) and minimal radioactive background. One of the most promising locations on the Moon for a neutrino telescope is the south pole of the Moon (Fig. 2). The lunar south pole features a region with crater rims exposed to near-constant solar illumination, yet the interior of the craters are permanently shaded from sunlight.

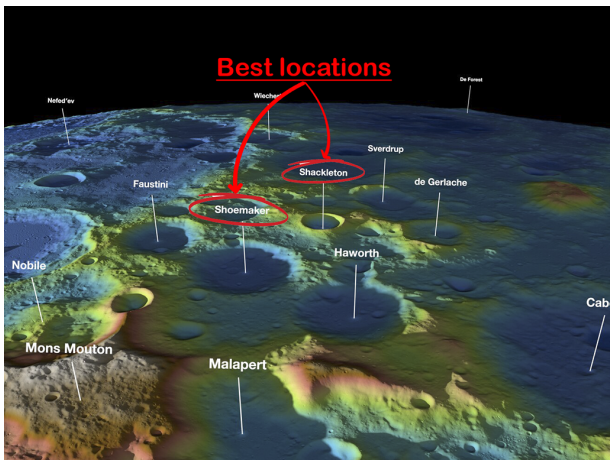

FIG. 2: Location of optimal craters on the Moon's surface.

The most promising candidate is the Shackleton crater. This crater is located in the southern hemisphere of the Moon and has a size of 130 km2 with the depth of about 4.2 km. The Shackleton crater is of interest for a neutrino telescope for several reasons:

- Large thickness of regolith: The Shackleton crater has a thick layer of lunar regolith, which can provide the necessary protection against radioactive background and cosmic radiation.
- Low radioactive background: The south pole of the Moon has a relatively low level of radioactive background compared to other regions of the Moon, which is important for detecting neutrino interactions.
- Stable temperature: The Shackleton crater has a stable temperature, which is important for the operation of a neutrino telescope.
- Availability of resources: The south pole of the Moon has access to water ice, which can be used to produce fuel, oxygen, and other necessary resources.

The other promising candidate is the Shoemaker crater. While temperature here is not as stable

as in the Shackleton crater, it features a larger area of around 500 km^2, with around 170 km^2 region of permanent darkness.
The concept of the detector is a Grid of piezoelectric sensors (3) with 10-100 kHz bandwidth, able to detect acoustic waves, produced by the Askaryan effect. Assuming AE detection radius as around 10m [4], we assume the number of detectors as 3000 and 300000 for 1 km^2 and 100 km^2 detector area respectively.

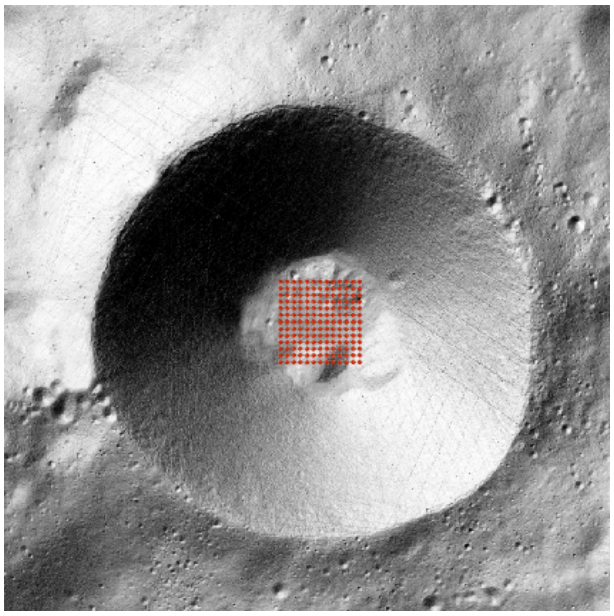

FIG. 3: Location of the piezoelectric sensor array inside the crater.

IV. NEUTRINO FLUX CALCULATION

The following parameterisation (IceCube-fit) was utilised to calculate the flux of neutrinos:

$$\frac{d\Phi_\nu}{dE} = 10^{-18} \left(\frac{E}{100 \text{ TeV}} \right)^{-2.3} \text{GeV}^{-1}\text{cm}^{-2}\text{s}^{-1}\text{sr}^{-1} \quad (3)$$

Moreover, it is feasible to get the integrated flux (E > 1 EeV):

$$\Phi_\nu \approx 10^{-16} \text{ cm}^{-2}\text{s}^{-1}\text{sr}^{-1} \quad (4)$$

Following a thorough and methodical process, a lower bound on the number of events per year was established:

$$N = \Phi_\nu \times S \times T \times \Omega \times \sigma \times \text{N}_{target} \times \text{L} \approx$$
$$\approx 10^{-16}\text{cm}^{-2}\text{s}^{-1} \times 10^{10}\text{cm}^2 \times 3 \times 10^7\text{s} \times$$
$$\times 2\pi \times 10^{-31}\text{cm}^2 \times 10^{23}\text{cm}^{-3} \times 10^5\text{cm} \approx \boxed{0.1 \text{ events}} \quad (5)$$

V. CONSTRUCTION PHASES AND EXPENDITURE BUDGET

Possible solutions to those include:

- Solar arrays at the crater rims (regions with permanent solar illumination);
- Passive radiators with phase-change materials;
- Multi-layer thermal insulation of equipment;
- Lossless data compression (1000:1 ratio);
- Lunar orbit relay constellation (up to 4 satellites).

Based on the above, we estimate budget expenditures as:

- **Phase 1** (Development): $50M over 5 years
  - Detector prototyping (30%)
  - Simulation studies (20%)
  - Technology maturation (50%)
- **Phase 2** (Deployment): $200M
  - Launch vehicle (60%)
  - Robotic deployment system (40%)
- **Phase 3** (Operations): $20M/year
  - Data analysis (40%)
  - Maintenance (30%)
  - Upgrades (30%)

VI. CONCLUSIONS

Building an observatory on Moons leads to the following technical challenges:

- power continuity;
- equipment thermal management;
- data transmission.

[1] B. L. Beron and R. Hofstadter. “Generation of Mechanical Vibrations by Penetrating Particles”. In: *Phys. Rev. Lett.* 23 (4 July 1969), pp. 184–186. DOI: 10.1103/PhysRevLett.23.184. URL: https://link.aps.org/doi/10.1103/PhysRevLett.23.184.

[2] G. A. Askarian et al. “ACOUSTIC DETECTION OF HIGH-ENERGY PARTICLE SHOWERS IN WATER”. In: *Nucl. Instrum. Meth.* 164 (1979), pp. 267–278. DOI: 10.1016/0029-554X(79)90244-1.

[3] L.D. Landau and E.M. Lifshitz. *Fluid Mechanics: Landau and Lifshitz: Course of Theoretical Physics, Volume 6*. т. 6. Pergamon, 2013. ISBN: 9781483161044.

[4] Wladyslaw Henryk Trzaska et al. *Acoustic detection of neutrinos in bedrock*. 2019. arXiv: 1909.00417 [physics.ins-det]. URL: https://arxiv.org/abs/1909.00417.

Can Earth's Atmosphere Serve as the Largest Neutrino Detector?

Amir Enik[1], Sofiya Sokolova[2], Irina Ulanova[3],
Nafisa Valieva[4], Jiamin Wang[5], Elena Yuzhakova[6]

[1]*Lebedev Physical Institute,* [2]*JINR,* [3]*Flerov Laboratory of Nuclear Reactions,*
[4]*SPbU,* [5]*PandaX,* [6]*MEPhI*

Project Author:
Dmitri Naumov,
JINR

Scientific Advisor:
Vladimir Allakhverdyan,
JINR

Abstract

While traditional neutrino detectors rely on dense media like water or ice to ensure sufficient interaction rates, the Earth's atmosphere, despite its low density, covers a vast volume and area. From orbit, one can observe fluorescence or Cherenkov light from extensive air showers initiated by ultra-high-energy neutrinos or gamma rays. Additionally, the Earth itself can act as a shield, allowing only neutrinos to skim through and initiate detectable upward-going events.
Evaluate the viability of using Earth's atmosphere as a large-scale neutrino detector. Estimate interaction rates, compare with water-based detectors, and identify the energy regime where atmospheric detection becomes competitive. Propose a realistic orbital detection concept and defend it as a scientific mission.

I. TASK 1: ATMOSPHERE VS WATER AS DETECTION MEDIUM

A. The effective mass of the atmosphere

Formula for Calculating Atmospheric Mass

The mass of the atmosphere can be calculated as the integral of air density over height:

$$M = \int_0^h 4\pi\rho(z)(R+z)^2 dz \qquad (1)$$

Where:

- $\rho(h)$ is the air density at height h (in kg/m^3),
- R is the radius of the Earth if we suppose that the Earth is an ideal sphere,
- $4\pi \cdot (R+z)^2$ is the surface area of the sphere,
- h is the upper boundary of the considered atmosphere (10 km in this case).

Simplifying the Calculation

Air density decreases with height according to an exponential law:

$$\rho(h) = \rho_0 e^{-\frac{gh}{RT_0}} \qquad (2)$$

Where:

- $\rho_0 = 1.225$ kg/m^3 is the air density at sea level,
- h - height,
- T_0 - temperature at sea level,
- R - specific gas constant for dry air,
- g - is the acceleration due to gravity.

Substitute the density formula into the integral:

$$M = A \int_0^h \rho_0 e^{-\frac{h}{H}} dh \tag{3}$$

Calculating the Integral

The integral of the exponent is calculated as:

$$\int e^{-\frac{h}{H}}\, dh = -He^{-\frac{h}{H}} \tag{4}$$

Substitute this into the formula:

$$M = A\rho_0 \left[-He^{-\frac{h}{H}}\right]_0^h \tag{5}$$

After simplification:

$$M = A\rho_0 H \cdot \left(1 - e^{-\frac{h}{H}}\right) \tag{6}$$

Substituting Values

- $A = 5.1 \times 10^{14}$ m^2,
- $\rho_0 = 1.225$ kg/m^3,
- $H = 8.5$ km $= 8500$ m,
- $h = 10$ km $= 10000$ m.

Substitute:

$$M = 5.1 \times 10^{14} \times 1.225 \times 8500 \left(1 - e^{-\frac{10000}{8500}}\right) \tag{7}$$

Calculation

1. First, the exponent:

$$e^{-\frac{10000}{8500}} = e^{-1.176} \approx 0.308 \tag{8}$$

2. Substitute the result:

$$M = 5.1 \times 10^{14} \times 1.225 \times 8500 (1 - 0.308) \tag{9}$$

3. Perform multiplication:

$$M = 5.1 \times 1.225 \times 8500 \times 0.692 \times 10^{14} \tag{10}$$

4. Result:

$$M \approx 3.7 \times 10^{18} \text{ kg} \tag{11}$$

Result

The effective mass of the atmosphere from sea level to 10 km is approximately 3.7×10^{18} kg.

B. Comparison with Water

For comparison, the mass of water in 1 km^3 (the volume of a standard water detector) is:

$$M_{\text{water}} = \rho_{\text{water}} V = 1000 \text{ kg/m}^3 \times 10^9 \text{ m}^3 = 10^{12} \text{ kg} \tag{12}$$

The atmosphere has a much larger mass, but its density is significantly lower, affecting the probability of neutrino interactions. One can compute neutrino interaction probability as particle flux times density of the target times the cross section of the interaction.
The column density N of a medium is given by the product of the density ρ and the thickness d of the medium: $N = \rho d$
The probability P of a neutrino interaction is then given by: $P = \sigma N = \sigma \rho d$, where σ - the cross-section for the neutrino interaction.
Let's assume, that the thickness of the atmosphere d is approximately 100 km and the cross-section for neutrino interactions σ is approximately $10^{-38} m^2$. So, then

$$N = \rho d = 1.225 \text{ kg/m}^3 \times 10^5 \text{ m} = 1.225 \times 10^5 \text{ kg/m}^2 \tag{13}$$

For air, the number of particles per kilogram is approximately $1.3 \cdot 10^{25}$ particles/kg:

$$\sigma N = 1.225 \times 10^5 \text{ kg/m}^2 \times 1.3 \times 10^{25} \text{ partilces/kg} = \\ = 1.5925 \cdot 10^{30} \text{ particles/m}^2 \tag{14}$$

$$P = \sigma N = \\ = 1.5925 \times 10^{30} \text{particles/m}^2 \times 10^{-38} m^2 = \\ = 1.5925 \times 10^{-8} \tag{15}$$

So, the probability of a neutrino interaction in the atmosphere is approximately 1.6×10^{-8}

II. COMPARING NEUTRINO INTERACTION PROBABILITIES IN WATER VS. ATMOSPHERE

A. Key Parameters

TABLE VI. Comparison of water and atmosphere parameters

Parameter	Water	Atmosphere
Density (ρ)	1 g/cm^3 = 10^3 kg/m^3	1.2 kg/m^3 (at sea level)
Effective path (L)	1 km (detector scale)	30 km (atmospheric height)
Cross-section (σ_ν)	$\sim 10^{-32}$ cm^2 (for E_ν = 10^{17}-10^{18} eV)	Same as water

B. Atomic Number Density (n)

$$n = \frac{\rho}{m_{\text{molecule}}} N_A \tag{16}$$

where $N_A = 6.022 \times 10^{23}$ mol^{-1} is Avogadro's number.

- **Water** (H_2O, molar mass $\approx$ 18 g/mol):

$$n_{\text{water}} = \frac{10^3 \text{ kg/cm}^3}{18 \times 10^{-3} \text{ kg/mol}} \times 6.022 \times 10^{23} \approx \approx 3.34 \times 10^{22} \text{ molecules/cm}^3 \tag{17}$$

- **Atmosphere** (air, avg. molar mass $\approx$ 29 g/mol):

$$n_{\text{air}} = \frac{1.2 \text{ kg/cm}^3}{29 \times 10^{-3} \text{ kg/mol}} \times 6.022 \times 10^{23} \approx \approx 2.48 \times 10^{19} \text{ molecules/cm}^3 \tag{18}$$

C. Optical Depth (τ)

$$\tau = n \cdot \sigma_\nu \cdot L$$

- **Water** (L = 1 km = 10^5 cm):

$$\tau_{\text{water}} = 3.34 \times 10^{22} \times 10^{-32} \times 10^5 \approx 3.34 \times 10^{-5} \tag{19}$$

- **Atmosphere** (L = 30 km = 3×10^6 cm):

$$\tau_{\text{air}} = 2.48 \times 10^{19} \times 10^{-32} \times 3 \times 10^6 \approx 7.44 \times 10^{-8} \tag{20}$$

D. Interaction Probability (P)

$$P = 1 - e^{-\tau} \approx \tau \quad (\text{for } \tau \ll 1) \tag{21}$$

- **Water**:

$$P_{\text{water}} \approx 3.34 \times 10^{-5} \quad (\approx 3.34 \times 10^{-3}\,\%) \tag{22}$$

- **Atmosphere**:

$$P_{\text{air}} \approx 7.44 \times 10^{-8} \quad (\approx 7.44 \times 10^{-6}\,\%) \tag{23}$$

E. Comparison & Conclusions

- Water offers **448 times higher** interaction probability per unit path (1 km)
- Atmosphere compensates with its vast volume (orbital detectors observe $\sim 10^5$ km^3)
- **For $E_\nu < 10^{17}$ eV**: Water is superior due to density
- **In the range $10^{17} - 10^{18}$ eV (100 PeV - 1 EeV)**: The atmosphere becomes comparable to large water-based detectors like IceCube. At these energies, the effective interaction volume of the atmosphere, when scaled against its lower density, can match the sensitivity of a cubic-kilometer water detector. The interaction cross-section, although still rising, shows initial signs of deviation from strict linearity.
- **For $E_\nu > 10^{19}$ eV**: Atmosphere becomes competitive due to rising σ_ν and large volume

III. TASK 2: NEUTRINO AND GAMMA-RAY DETECTION MODES

A. Down-going Neutrinos or Gamma Rays

Physical Process

- A neutrino or gamma-ray enters the Earth's atmosphere from above.
- Gamma rays initiate electromagnetic cascades; neutrinos interact via weak interactions, producing hadronic or electromagnetic air showers.
- These showers propagate downward and generate secondary particles.

Observational Signatures

- **Fluorescence Track:** Excited nitrogen molecules emit UV light along the shower path. The result is a long, track-like signal visible at night under clear atmospheric conditions. Detectors: *Pierre Auger, POEMMA, EUSO*.
- **Cherenkov Flash:** A sharp, forward-directed blue light flash from relativistic electrons in the shower. Very brief (nanoseconds). Can be detected from the ground, balloon platforms, or orbit if aligned. Detectors: *Ashra, Trinity*.

- **Surface Particles:** Secondary particles that reach the ground (muons, electrons) can be detected using surface arrays. Detectors: *IceTop, Auger, Telescope Array*.

Signal Properties

- Duration: nanoseconds (Cherenkov) to microseconds (fluorescence)
- Direction: downward
- Spatial distribution: from narrow beam to extended track

B. Earth-skimming ν_τ Neutrinos

Physical Process

- ν_τ enters the Earth at a shallow angle and interacts in rock or crust, producing a tau lepton.
- The tau lepton exits the Earth and decays in the atmosphere, initiating an upward-moving air shower.

Observational Signatures

- **Upward-going Cherenkov Flash:** A narrow beam of Cherenkov light emitted near the horizon, traveling upward. This is a unique signal to ν_τ and provides excellent background suppression. Detectors: *ANITA, BEACON, Trinity*.
- **Fluorescence from Upward Shower:** Similar to standard fluorescence tracks, but moving upward. Visible from orbital or mountain-based platforms. Detectors: *POEMMA (planned)*.

Signal Properties

- Duration: nanoseconds (Cherenkov), microseconds (fluorescence)
- Direction: upward, near the horizon
- Uniqueness: only ν_τ can produce this signal

TABLE VII. Comparison of Neutrino Detection Modes

Feature	Down-going	Earth-skimming
Shower Direction	Downward	Upward
Type of Neutrino	Any ν, γ	ν_τ
Observable Signatures	Fluorescence, Cherenkov, surface arrays	Cherenkov, fluorescence from horizon
Event Probability	Higher	Lower
Signal Uniqueness	Low (background from cosmic rays)	High (unique upward-going shower)
Direction	From above	Near-horizontal (from Earth)
Interaction Site	In the atmosphere	In Earth's crust
Energy Range	10^{17}–10^{19} eV	$> 10^{17}$ eV
Example Projects	Auger, EUSO, POEMMA	ANITA, Trinity, BEACON, POEMMA

IV. CONCLUSION

- **Mode 1:** Suitable for mass neutrino observation but requires complex technology for background suppression.
- **Mode 2:** Unique for studying ultra-high-energy neutrinos, especially tau neutrinos, and could be key for orbital detectors.

V. OBSERVATIONAL SIGNATURES OF NEUTRINO AND GAMMA-RAY DETECTION MODES

This section describes in detail the observational signals produced in the two main detection modes of ultra-high-energy (UHE) neutrinos and gamma rays in the atmosphere.

VI. COMPARISON TABLE OF OBSERVATIONAL SIGNATURES

TABLE VIII. Comparison of Detection Features for Down-going and Earth-skimming Neutrinos

Feature	**Comparison: Down-going (ν, γ) vs Earth-skimming (ν_τ)**
Main Signal	Fluorescence, Cherenkov, surface particles vs Upward Cherenkov, fluorescence
Shower Direction	Downward vs Upward, near-horizontal
Signal Duration	ns–μs vs ns–μs
Detection Platforms	Ground, orbital vs Balloon, orbital, mountaintop
Signal Uniqueness	Not unique vs Unique to ν_τ
Viewing Conditions	Night-time, clear sky vs Horizon visibility, low background

VII. TASK 3: RATE ESTIMATES

A. Objective

Estimate the expected number of ultra-high-energy (UHE) neutrino events per year that can be observed from space, given a specific neutrino flux model and assuming a reasonable field of view for the detector.

B. General Formula

The expected number of events N per year is calculated using the following expression:

$$N = \Phi(E) \cdot \sigma(E) \cdot \rho \cdot A_{\text{eff}} \cdot L \cdot T \cdot \Omega_{\text{eff}} \cdot N_A \quad (24)$$

Where:

- $\Phi(E)$ is the neutrino flux for energies above 10^{19} eV,
- $\sigma(E)$ is the neutrino interaction cross-section at 10^{10}GeV,
- ρ is a density of the Earth crust,
- A_{eff} is the effective area of the detector (cm²),
- L is a livetime fraction,
- T is the total observation time,
- Ω_{eff} is a solid angle,
- N_A - an Avogadro number.

C. Detector Parameters

We assume a space-based detector with:

$$A_{\text{eff}} = 1 \times 10^{16}\,\text{cm}^2 \quad (25)$$

Field of view FoV is from $5°$ to $10°$. The corresponding solid angle Ω_{eff} is 0.1 sr.
Observation time:

$$T = 3.15 \times 10^7\,\text{s/year} \quad (26)$$

Realistic GZK neutrino flux:

$$\Phi_0 = 1 \times 10^{-18}\,\text{eV}^{-1}\text{cm}^{-2}\text{s}^{-1}\text{sr}^{-1} \quad (27)$$

D. Calculations

$$N = \Phi(E) \cdot \sigma(E) \cdot N_{\text{scattering}} T \cdot \Omega_{\text{eff}} \quad (28)$$

$$N_{\text{scattering}} = N_{\text{nucl.}} = A \cdot N_{\text{atoms}} = \\ = A \cdot \nu \cdot N_A = A \cdot \frac{m}{M} \cdot N_A = m \cdot N_A \quad (29)$$

$$m = \rho \cdot V = \rho \cdot A_{\text{eff}} \cdot L \quad (30)$$

$$N = \Phi_0 \cdot \sigma \cdot \rho \cdot A_{\text{eff}} \cdot L \cdot T \cdot \Omega_{\text{eff}} \cdot N_A \quad (31)$$

- $\Phi_0 = 1 \times 10^{-18}\,\text{eV}^{-1}\text{cm}^{-2}\text{s}^{-1}\text{sr}^{-1}$ - neutrino flux,
- $\sigma = 10^{-32}\text{cm}^2$ - cross-section of neutrino interaction,
- $\rho = 2.8\frac{\text{g}}{\text{cm}^3}$ - the density of the Earth crust,
- $N_A = 6 \times 10^{23}\text{mole}^{-1}$ - an Avogadro number

- $A_{\text{eff}} = 10^{16}\text{cm}^2$ - an effective detector's area,
- $L = 2 \times 10^5$ cm - an effective interaction length,
- $\Omega_{\text{eff}} = 0.1$sr - a solid angle,
- $T = 3.15 \times 10^7$s - seconds in a year.

E. Final Result

$$\boxed{N \approx 11 \text{ events per year}}$$

F. Conclusion

This is a first-order estimate of the number of UHE neutrino events observable from space in one year using a detector with $A_{\text{eff}} = 10^{16}\,\text{cm}^2$ and a field of view from $5^\circ \times 10^\circ$, assuming a simple GZK flux model. More accurate estimates would include energy-dependent effective areas and detailed simulation of interaction probabilities and atmospheric geometry.

VIII. COMPARISON WITH ICECUBE AND OTHER DETECTORS

A. Objective

Compare the previously estimated event rate for a space-based ultra-high-energy (UHE) neutrino detector with expected rates from large-scale ground-based neutrino observatories such as IceCube.

B. IceCube Overview

IceCube is a large-volume neutrino telescope located at the South Pole, utilizing a cubic kilometer of Antarctic ice to detect neutrino interactions. It is optimized for detecting astrophysical neutrinos with energies ranging from a few TeV up to several PeV and beyond.

C. Expected Rates in IceCube

- **Cosmogenic (GZK) Neutrinos:** The expected event rate for cosmogenic neutrinos in IceCube is approximately **1 event per year** for energies above 10^{18} eV (1 EeV), depending on the flux model.
- **Atmospheric Background:** At energies above 10^{14} eV (100 PeV), the rate of atmospheric background events is extremely low, on the order of 10^{-5} events per year.
- **Astrophysical Neutrinos:** IceCube has observed a diffuse flux of astrophysical neutrinos with energies up to a few PeV, but the number of events with energies above 10^8 GeV remains very limited.

D. Comparison of Key Factors

Effective Area

- **IceCube:** The instrumented volume corresponds to an effective area of approximately 10^{10} cm^2 for high-energy neutrinos.
- **Space-Based Detector (Our Estimate):** The effective area used in our calculation was $A_{\text{eff}} = 10^{16}$ cm^2 (10^6 km^2), which is much larger.

Field of View

- **IceCube:** Limited to observing neutrinos coming through or near the horizon. The solid angle is typically below 1 sr for UHE neutrinos.
- **Space-Based Detector:** In our model, the detector observes with a field of view from 5° to 10°, corresponding to an effective solid angle of approximately 0.1 sr. Space-based observatories can monitor a significantly larger portion of the atmosphere, leading to higher detection potential.

Energy Sensitivity

- **IceCube:** Optimized for the TeV–PeV energy range. Sensitivity to EeV-scale neutrinos is limited due to the small interaction cross-section and Earth absorption.
- **Space-Based Detector:** Designed to target neutrino interactions in the upper atmosphere, and thus more sensitive to EeV and ZeV neutrinos. From orbit, the detector can see nearly horizontal or Earth-skimming events, which are rare in IceCube.

E. Interpretation and Conclusion

The estimated rate of approximately 11 events per year for the space-based detector significantly exceeds the expected rate in IceCube for cosmogenic neutrinos. This discrepancy can be explained by:

- The larger observable target volume (Earth's atmosphere) from orbit.
- The larger effective area.
- The energy range being optimized for ultra-high-energy interactions.

However, this theoretical estimate assumes ideal conditions and a constant effective area. Real detection rates depend on numerous factors including the detection efficiency, energy resolution, background rejection, and angular acceptance.
Future comparisons should also include next-generation detectors such as IceCube-Gen2, POEMMA, and GRAND, which are designed to improve sensitivity to the cosmogenic neutrino flux.

IX. TASK 4. MISSION DESIGN

A. Detection system. Detector P10

P10 consists of two identical satellites flying in formation. This allows them to observe overlapping areas on moonless nights, at angles from the nadir to just above the edge of the Earth. The altitude of the satellites is planned to vary in tandem, from about 525 kilometers to 1000 kilometers. Different separation and guidance strategies will be used.
Each satellite will be equipped with Schmidt Telescopes with 6.5 m diameter mirrors and a Cherenkov Camera based on silicon photomultipliers (SiPM) to detect Cherenkov radiation occupying the full focal surface. Protective systems: movable cover to protect against stray light and micrometeorites. Calibration lasers for checking the transparency of the atmosphere and an IR camera for calibrating mirrors.

B. Detection principle

Tau neutrinos interact with the Earth's nuclei, giving birth to tau leptons, which decay in the atmosphere. Tau-lepton decay generates an ascending atmospheric shower accompanied by Cherenkov radiation. Our orbital detector will be able to detect cosmogenic tau neutrinos by observing Cherenkov radiation produced by ascending tau decays (observation of rising showers).

C. Coverage area

The satellites are at an altitude of 1000 km, the distance between them is 50 km. Observation area: an area at a distance of $3,700$ km from the satellites (Earth's limb). Field of view $5-10°$ to capture Cherenkov radiation.
The effective area will be equal to the geometric area that the detector sees $S_g\cdot$ the probability of registration. The geometric area is the area of a circle with a radius of $L/2$, L in our case 1000 km, then $S_g = \pi \cdot 500^2 = 7.85 \cdot 10^5 \text{km}^2$. We have good detectors and a quantum sensitivity of 40% SiPM and 40% light loss in the atmosphere. Then the total probability of registration is 0.25. Hence the effective area of the detector $S_{eff} = S_g \cdot 0.25 = 7.85 \cdot 10^5 \cdot 0.25\,\text{km}^2 = 2 \cdot 10^5\,\text{km}^2$.
Then the overlap is the effective area × solid angle × detector operating time (let's take 4.5 years, taking into account the illumination from the moon). Total $2 \cdot 10^5 \text{km}^2 \cdot 0.1\text{sr} \cdot 4.5\text{years} = 9 \cdot 10^4 \text{km}^2\text{sr year}$.

D. Expected sensitivity

Detection of cosmogenic tau neutrinos in the range $1-10$ EeV (peak of the GZK effect). Detector coverage is 10^4 km^2 · cp · year, expected GZK neutrino flux (in the range $1-10$ EeV): 0.1–1 event/year km^2 [1], with 5 years of work: 0.5–5 events will be sufficient for statistically significant detection.

E. Background suppression strategies

Stereoscopic verification: matching signals from two satellites eliminates false events.
Temporary resolution: SiPMs with a sampling time of 100 ns make it possible to separate fast Cherenkov signals from the background glow of the atmosphere. Geometric filtering: Observing only ascending showers (from Earth into space), which excludes 99% of background events (for example, atmospheric showers from cosmic rays).
Waveform analysis: Cherenkov light has a characteristic temporal structure (short pulse), which distinguishes it from scattered background radiation. It is planned to isolate the signals using a matching system from two satellites, and with a good time resolution (100 ns), the slow glow of the background will be eliminated. At a further stage of processing, we will select events only from ascending showers, we can use neural networks to analyze images, since the image from vertical showers will give a different illumination.

X. TASK 5. BUDGET AND PROPOSAL DEFENSE

1. **Design (2025-2028)**
   Modeling and testing: Testing of sensitivity to Cherenkov radiation in vacuum chambers. Creation of a 6.5 m prototype mirror for ground testing.
   Orbital mechanics: Calculation of the optimal configuration of satellites.

2. **Construction (2029-2032)**
   Manufacturing of components: Production of mirrors with protective coating. Assembly of SiPM cameras with radiation-resistant electronics.

System integration: Installation of calibration lasers and IR cameras. Testing of protective mechanisms (caps, movable caps).
Ground tests: Simulation of space conditions (temperature, vibrations, radiation).

3. **Launch (2033)**
Launch vehicle: Falcon Heavy or similar (double launch).
Orbit: Circular, altitude 1000 km, inclination 28.5°.
Deployment: Separation of satellites, opening of mirrors, solar panels, antennas.
Test phase: calibration of cameras, verification of communication between satellites.

4. **Operation (2033-2038)**
Scientific operations: Observation of the Earth's limb for 90% of the time (moonlit nights are excluded), although it is possible not to exclude moonlit nights because silicon power plants can work on moonlit nights, just the background will increase.
Data collection on Cherenkov events with a frequency of $\sim$ 1 TeV/day. An example of a data acquisition device: silicon photomultipliers (SiPMs) with high read speed, ASIC chips for real-time signal processing, solid-state drives (SSDs) for data storage, and laser/radio communications for data transmission to Earth Calibration and monitoring: Monthly guidance accuracy check using onboard lasers.
Correction of the orbit to maintain the formation. Data analysis: Isolation of tau neutrino signals against the background of atmospheric and cosmic noise.

A. Approximate cost estimate in rubles

Stage Cost (billion RUB), cost with increased margin for costs

- **Design - 160**
The cost of designing a mirror for the JWST telescope is \$1.5 billion (about 135 billion rubles, adjusted for inflation) [2]. For the P10, it has a smaller scale and localization in the Russian Federation, which reduces costs. Calculation of the satellite configuration. Example: ESA spends $10 - 20$ million euros on similar tasks for LISA class missions [3].

- **Construction – 40**
6.5-m mirrors with protective coating. The cost of one mirror is 15 billion rubles (equivalent: E-ELT mirrors — \$40 million/piece)[**eso**]. Silicon photomultipliers (SiPM) 2 million rubles/m2. For two satellites 8 billion rubles [**sipm**]. Radiation-resistant electronics: 5 billion rubles. (based on prices of "Russian Space Systems"). Lasers, IR cameras 3 billion rubles.

- **Launch – 18**
Double launch on Falcon Heavy — \$180 million (≈16 billion rubles). Additional expenses (adaptation, insurance) — 2 billion rubles [4]. The alternative: Angara-A5 — 7 billion rubles./launch, but two satellites will require two launches (14 billion rubles) + a reserve [5].

- **Operation (5 years) – 10**
Orbit correction — 1 billion rubles/year (equivalent: support for GLONASS satellites — 0.8–1.2 billion rubles/year) [5]. Processing center (server rental, software) — 0.5 billion rubles/year. Laser systems, IR cameras —0.2 billion rubles/year.

Approximate total amount: 228 billion rubles.

XI. SUMMARY OF THE PROPOSAL

A. Why watch from space?

Large coverage area: Space detectors observe 70% of the Earth's atmosphere, which is unattainable for ground-based observatories.
Minimum background: Absence of atmospheric absorption of UV radiation and interference from urban illumination.
Access to rising showers: Tau neutrinos interacting with the Earth can be detected only from space.

B. Why use the atmosphere?

The advantage of a natural detector is that the Earth serves as a target for neutrinos, and the Cherenkov radiation in the atmosphere from tau leptonite decays is an indicator of events. Also, ground-based detectors cannot register rising showers (at least with high accuracy), since they are directed into space.

C. Why is it worth the investment?

A breakthrough in astrophysics: The detection of GZK neutrinos will confirm theories about the origin of UHECR and the properties of neutrinos at energies $>$ 1 EV. Neutrinos are also the only particles capable of passing through intergalactic media without distortion.
There is a technological benefit: The development of radiation-resistant SiPMs and large-size mirrors for space stimulates innovation.
Bottom line: The mission will provide unique data on the most energetic processes in the universe without distortion by galactic magnetic fields.

XII. CONCLUSION

This project investigates the potential of using Earth's atmosphere as a large-scale neutrino detector, particularly for ultra-high-energy neutrinos arising from cosmogenic sources. Despite its low density, the atmosphere offers an immense observational volume that can compensate for its weaker interaction probability compared to dense media like water or ice. Our analytical and numerical results show that, above energies of 10^{17} eV, the atmosphere becomes a competitive detection medium, and beyond 10^{19} eV, it may outperform traditional ground-based detectors, especially when observed from space. We examined key detection modes, including down-going and Earth-skimming tau neutrinos, and showed that the latter produce unique upward-going air showers that are best observed from orbit. Based on realistic cosmogenic neutrino flux models, we estimate that a 10^6 km^2 orbital detector with a from 5° to 10° field of view could detect around 11 events per year. We proposed a mission concept involving two satellites with wide-field Schmidt telescopes and SiPM-based Cherenkov cameras, capable of stereoscopic observation and background suppression. These findings support the feasibility of orbital neutrino astronomy and highlight the scientific value of detecting ultra-high-energy neutrinos as probes of the most extreme processes in the universe.

---

[1] O. Adriani et al. "The ultra-high-energy event KM3-230213A within the global neutrino landscape". In: (Feb. 2025). arXiv: 2502.08173 [astro-ph.HE].

[2] URL: https://www.esa.int/.

[3] URL: https://science.nasa.gov/mission/webb/.

[4] URL: https://www.spacex.com/.

[5] URL: https://www.roscosmos.ru/.